Drug Design, Development and Therapy

Dovepress
Taylor & Francis Group

Open Access Full Text Article

ORIGINAL RESEARCH

Huashi Jiedu Decoction Enhances 5-Fluorouracil Efficacy in Gastric Cancer via miRNA-21-3p/p53 Pathway

Qianran Hong[1], Weiye Lin[1], Yici Yan[1], Shuangyu Chen[1], Jiayang Li[1], Jieru Yu[2], Ying Zhu[3], Shengliang Qiu[1]

[1]The First Affiliated Hospital of Zhejiang Chinese Medical University (Zhejiang Provincial Hospital of Chinese Medicine), Hangzhou, Zhejiang, 310006, People's Republic of China; [2]School of Basic Medical Sciences, Zhejiang Chinese Medical University, Hangzhou, Zhejiang, People's Republic of China; [3]Department of Medical Oncology, The First Affiliated Hospital of Zhejiang Chinese Medical University (Zhejiang Provincial Hospital of Chinese Medicine), Hangzhou, Zhejiang, People's Republic of China

Correspondence: Ying Zhu, Department of Medical Oncology, The First Affiliated Hospital of Zhejiang Chinese Medical University (Zhejiang Provincial Hospital of Chinese Medicine), Hangzhou, People's Republic of China, Email ying.zhu@zcmu.edu.cn; Shengliang Qiu, The First Affiliated Hospital of Zhejiang Chinese Medical University (Zhejiang Provincial Hospital of Chinese Medicine), Hangzhou, Zhejiang, 310006, People's Republic of China, Email shengliang.qiu@zcmu.edu.cn

Purpose: To explore the mechanism of Huashi Jiedu Decoction (HJD) synergizing with 5-fluorouracil (5-Fu) in gastric cancer (GC) therapy.

Methods: MicroRNAs (miRNAs) and genes involved in HJD-mediated GC treatment were identified using ultra-high-performance liquid chromatography coupled with quadrupole-Orbitrap mass spectrometry, network pharmacology, Gene Ontology, Kyoto Encyclopedia of Genes and Genomes, and molecular docking. The effects of HJD on 5-Fu sensitivity in BGC-823 cells were evaluated with 3-(4,5-Dimethylthiazol-2-yl)-2,5-diphenyltetrazolium bromide assays, reverse transcription quantitative polymerase chain reaction (RT-qPCR), and Western blotting. Synergistic effects in vector-transfected and miRNA-21-3p knockdown cells were assessed by colony formation, wound healing, transwell assays, and flow cytometry (FCM). An in vivo study evaluated the impact of HJD on 5-Fu sensitivity, measuring miRNA-21-3p, tumor protein p53 (p53), N-cadherin, vimentin, and E-cadherin in tumors, along with tumor volume and weight.

Results: miRNA-21-3p and p53 were key targets in HJD's therapeutic effect on GC. RT-qPCR showed that HJD combined with 5-Fu reduced miRNA-21-3p and upregulated p53 in vector cells and increased p53 mRNA ($p < 0.01$) and protein ($p < 0.05$) compared to 5-Fu alone. These effects were abolished in miRNA-21-3p knockdown cells. The combination reduced colony formation by 48.92% ($p < 0.01$), suppressed transwell migration by 28.5% ($p < 0.01$), and inhibited wound healing by 81.9% compared to 5-Fu monotherapy ($p < 0.001$), with no effects in knockdown cells. FCM showed a 15.1% increase in G_0/G_1 phase arrest ($p < 0.05$). In vivo, the combination significantly reduced tumor volume ($p < 0.05$) and weight by 18.7%, with concomitant miRNA-21-3p downregulation ($p < 0.0001$), EMT marker suppression (N-cadherin, vimentin), and tumor suppressor activation (p53, E-cadherin) versus 5-Fu alone.

Conclusion: HJD enhances 5-Fu's effects on GC by regulating the miRNA-21-3p/p53 pathway and modulating cadherin expression, supporting its potential as an adjunctive treatment in GC.

Keywords: huashi jiedu decoction, 5-fluorouracil, gastric cancer, miRNAs, p53

Introduction

Gastric cancer (GC) is a highly heterogeneous disease with over one million new cases diagnosed annually, accounting for 7.8% of global cancer-related fatalities.[1] Combination chemotherapy regimens based on 5-fluorouracil (5-Fu) are the most commonly used treatments for patients with GC with high levels of malignancy or contraindications to surgery worldwide.[2] However, patients often develop intrinsic and acquired resistance during chemotherapy, leading to variability in drug sensitivity and poor treatment outcomes.[2] The five-year survival rate remains at a mere 35.9%.[3]

Traditional Chinese medicine (TCM) has recently gained attention as a complementary therapy for GC, particularly for its ability to enhance tumor responsiveness to chemotherapeutic agents through multi-target mechanisms.[4] For

Received: 26 January 2025
Accepted: 9 May 2025
Published: 15 May 2025

Graphical Abstract

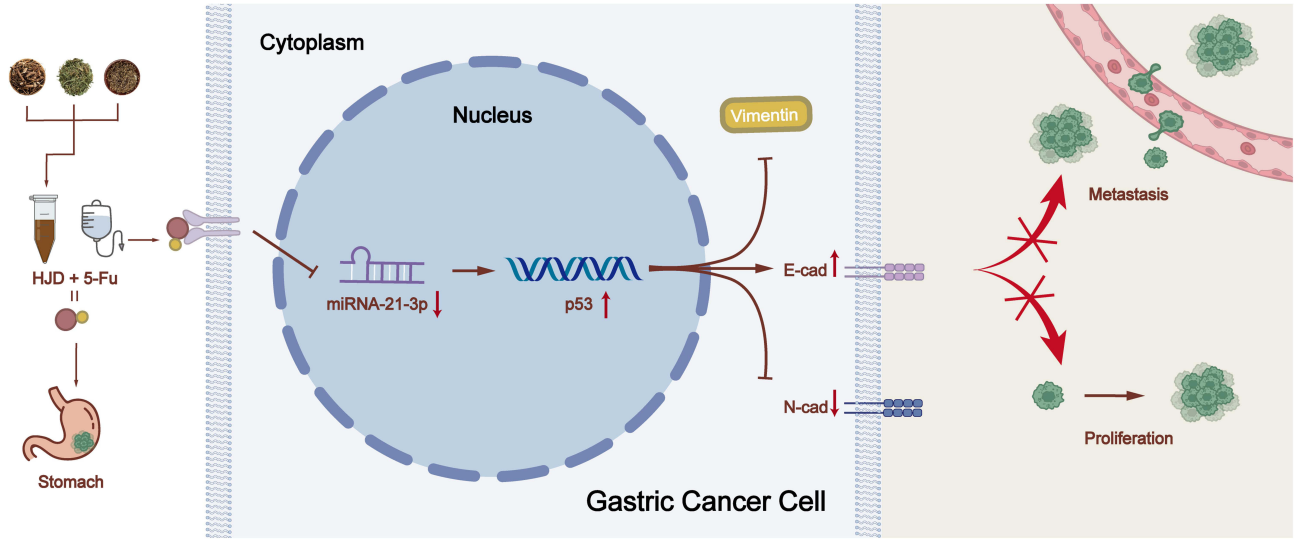

instance, Yiqi Huayu Jiedu Decoction has been demonstrated to reverse chemoresistance in GC by modulating the protein kinase B (AKT)/glycogen synthase kinase 3 beta/nuclear factor erythroid 2-related factor 2/glutathione peroxidase 4 axis,[5] while Jianpi Huatan Formula exerts its chemosensitizing effects through the phosphoinositide 3-kinase/AKT/mechanistic target of rapamycin pathway.[6] Huashi Jiedu Decoction (HJD) is composed of equal proportions of Hedyotis diffusa Spreng (HD), Patrinia villosa Juss. (HP), and Rabdosia amethystoides (Benth). H.Hara (HRA). In TCM, HD is primarily used to clear heat and detoxify; HP is effective in expelling pus and promoting blood circulation; and HRA is known for its ability to invigorate blood and alleviate dampness. The combination of these three herbs works synergistically to clear damp-heat and resolve stasis-toxins in GC, which is conceptually consistent with the principles of tumor microenvironment regulation in contemporary medical research. Previous research has suggested that HJD inhibits GC cell migration and invasion by downregulated long non-coding RNA *p21*.[7] However, whether HJD enhances the inhibitory effects of 5-Fu on GC remains unclear, particularly regarding its potential to modulate molecular regulators of chemoresistance, such as miRNAs.

MicroRNAs (miRNAs), approximately 20 nucleotides in length, exert extensive regulatory effects on target genes and participate in 5-Fu resistance mechanisms in GC.[8,9] For example, miRNA-139-3p acts as a pivotal regulator of 5-Fu resistance in GC, and its downregulation in GC tissues is associated with compromised 5-Fu sensitivity.[10] Similarly, suppression of miRNA-506-3p elevates polypyrimidine tract-binding protein 1 expression, thereby inducing glycolytic reprogramming that sustains energy supply for 5-Fu-resistant GC cells.[11] Furthermore, overexpression of miRNA-877-3p activates the Janus kinase 2/signal transducer and activator of transcription 3 (JAK2/STAT3) signaling pathway, which enhances cancer stemness properties to counteract 5-Fu therapeutic efficacy in GC.[12] Notably, while the potential of Chinese herbal medicines in modulating miRNAs to overcome chemoresistance has been increasingly explored in recent studies,[13–15] research investigating how TCM compound decoctions upregulate 5-Fu resistance in GC through miRNA remains unexplored.

To address this gap, we investigated whether HJD synergizes with 5-Fu in GC and specifically focused on miRNA-21-3p/p53 pathway as a potential chemosensitization mechanism. The active components of HJD were identified using ultra-high-performance liquid chromatography coupled with quadrupole-Orbitrap mass spectrometry (UHPLC-Q-Orbitrap HRMS) and network pharmacology. Subsequently, bioinformatics analysis was performed to prioritize miRNA-21-3p and p53 as key targets. To validate the synergistic effects and underlying mechanisms, in vitro assays and in vivo xenograft models were employed, with further evaluation of epithelial-mesenchymal transition (EMT) markers and cell cycle regulation. The systematic scheme of this study has been illustrated in Figure 1.

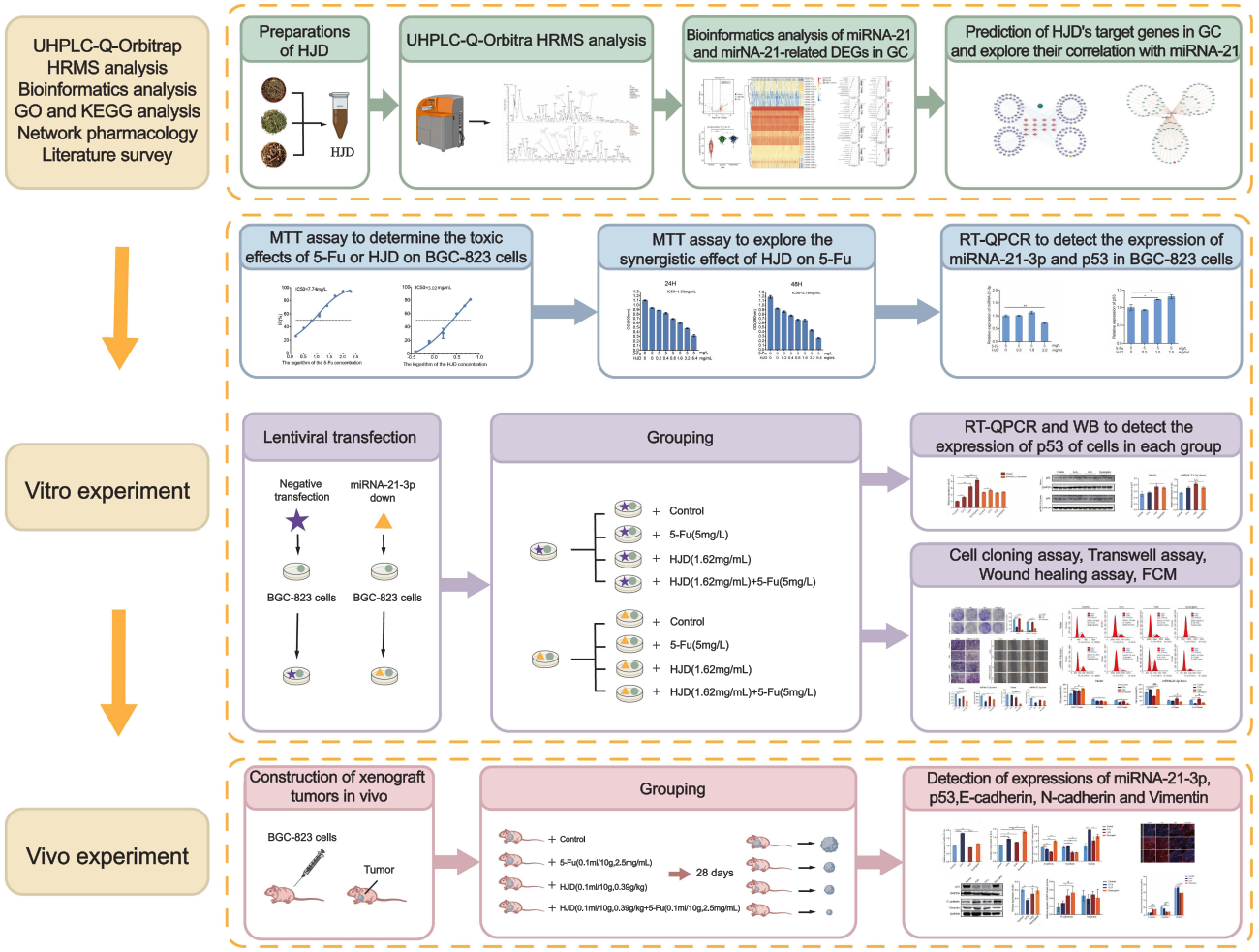

Figure 1 General experimental progress.

Materials and Methods

Drug, Reagents and Cell Line

Hedyotis diffusa Spreng (Zhejiang province, China, batch number 201401), Patrinia villosa Juss. (Zhejiang province, China, batch number 201301), and Rabdosia amethystoides (Benth). H.Hara (Zhejiang province, China, batch number 201501) were purchased from the First Affiliated Hospital of Zhejiang Chinese Medical University (Hangzhou, China). Human GC cell line BGC-823 was purchased from Shanghai Genechem Co., Ltd. (Shanghai, China) on 5 November 2018. 5-Fu injection (Southwest Pharmaceutical Co., Ltd., Chongqing, China, product number H50020128,) was brought from The First Affiliated Hospital of Zhejiang Chinese Medical University (Hangzhou, China). Lentiviral transfection negative vector and miRNA-21-3p knockdown vector were purchased from Shanghai Genechem Co (Shanghai, China). Primary antibodies against p53 (9282S), E-cadherin (3195S), N-cadherin (13116S), Vimentin (5741S), Glyceraldehyde-3-phosphate dehydrogenase (GAPDH) (2118S) were purchased from Cell Signaling Technology (Massachusetts, USA). Secondary antibodies Goat anti-Rabbit IgG (926–32211) was purchased from LI-COR Biosciences (Nebraska, USA). 3-(4, 5-Dimethylthiazol-2-yl)-2, 5-diphenyltetrazolium bromide (MTT) was obtained from Promega (Sigma-Aldrich, USA). Fetal bovine serum (FBS) was bought from Tianhang Biotechnology (Zhejiang, China). Roswell Park Memorial Institute-1640 (RPMI-1640) medium (containing 100 u/mL penicillin and 100 μg/mL streptomycin) was obtained from Senrui Biotechnology (Zhejiang, China). BALB/c nude mice (age 5 weeks) were brought from the Shanghai BK Laboratory Animal Company (Shanghai, China).

https://doi.org/10.2147/DDDT.S513371

Preparation of Extraction of HJD

The herbal composite (HD, HP, HRA; 1:1:1 ratio, 1.5 kg total) underwent dual decoctions (1 L distilled water per cycle, 100°C, 1.5 h/cycle). Combined extracts were sieved, centrifuged (3,000 rpm, 10 min), and lyophilized into bioactive powder (herb-to-powder ratio 62:1). For experimental use, the powder was reconstituted in cell culture medium (in vitro) or normal saline (NS) (in vivo).

Qualitative Analysis for HJD

Mass Spectrometry Conditions

The HJD decoction was analyzed using UHPLC-Q-Orbitrap HRMS (Thermo Fisher Scientific Co, Waltham, Massachusetts, USA). The conditions were as follows: ion source, electrospray ionization; scanning mode, positive and negative ion-switching; detection method, full mass spectrometry/data-dependent MS2; resolution, 17500; scan range, 100–1500 m/z; spray voltage, 3.2 kV (positive, negative); capillary temperature, 300 °C; collision gas, high-purity argon (purity ≥99.999%); sheath gas, nitrogen (purity ≥99.999%), 40 Arb; auxiliary gas and heater temperature, nitrogen (purity ≥99.999%), 350 °C; data collection time, 30.0 min.

Chromatographic Conditions

Chromatographic separation was performed using an Aqueous C18 column (150×2.1 mm, 1.8-μm particle size, Welch Materials, USA). The mobile phase flow rate was set to 0.3 mL/min, and the column and container were maintained at 35°C, while the sample tray was kept at 10°C. An automatic injector dispensed 5.00 μL of the sample. The mobile phase consisted of water with 0.1% formic acid (Phase A) and methanol (Phase B). The gradient elution program was as follows: 98% A + 2% B for 0–1 min, 80% A + 20% B for 1–5 min; 50% A + 50% B for 5–10 min; 20% A + 80% B for 10–15 min; 5% A + 95% B for 15–27 min; and returning to 98% A + 2% B for 27–30 min.

Collection of GC-Related miRNAs

The miRNAs exhibiting differential expression in GC were investigated by utilizing data sourced from UCSC XENA (https://xenabrowser.net/datapages/). We obtained 450 cases involving 40 normal cases and 410 GC cases. Differentially expressed miRNAs of GC were identified by "BiocManager" and "limma" R packages in R Studio (version R-4.3.3), and the details on cutoffs were as follows: $|\log FC| > 1.0$ and $p < 0.05$. The heatmap of differentially expressed miRNAs of GC was visualized by "ggplot2" and "pheatmap".

Bioinformatics Analysis of miRNA-21

The primary group was designated for stages I and II, and stages III and IV were categorized under the metastasis group, based on the National Health Service Cancer Grading guidelines (https://www.nhs.uk) and the American Joint Committee on Cancer classification criteria. We obtained 433 cases involving 41 normal cases, 180 primary cases, and 212 metastatic GC cases from the data of UCSC XENA (http://xena.ucsc.edu/getting-started/). The different expressions of miRNA-21 in normal tissues, primary stage GC tissues, and metastatic GC tissues were analyzed by using "tidyverse" and "edgeR" packages in R studio (version R-4.3.3). The clinicopathological characteristics and their relationship with miRNA-21 expression were collected and analyzed by the "tidyverse" and "stats" packages in R studio (version R-4.3.3).

Functional Enrichment Analysis in GC

By integrating the use of the data from UCSC XENA (http://xena.ucsc.edu/getting-started/) and the Genotype-Tissue Expression database (GETx) (https://getxinstitute.com/), we classified GC cases based on high and low expression levels of miRNA-21 using "tidyverse" R package in R Studio (version R-4.3.3). A total of 218 cases of GC with high miRNA21 expression, 218 cases of GC with low miRNA21 expression, and 214 normal cases were obtained. Differentially expressed genes (DEGs) in GC with high and low miRNA21 expression were identified by "BiocManager" and "limma" R packages in R Studio (version R-4.3.3) and the details on cutoffs were as follows: $|\log FC| > 1.0$ and $p < 0.05$. These DEGs were further subjected to Gene Ontology (GO) enrichment analyses, including biological processes (BPs), cellular components (CCs), and molecular functions (MFs), as well as Kyoto Encyclopedia of Genes and Genomes (KEGG) analyses on the David website (https://davidbioinformatics.nih.gov/). $p < 0.05$ was recognized as significant of GO Enrichment and KEGG

Enrichment. The graphical representation was created using a dedicated and publicly accessible online platform (https://www.bioinformatics.com.cn, last accessed on 10 November 2023).

Collection of GC-Related Gene Targets

The DEGs of GC were analyzed by using the combination of data from UCSC XENA (http://xena.ucsc.edu/getting-started/) and the Genotype-Tissue Expression database (GETx) (https://getxinstitute.com/). We obtained 500 cases involving 83 normal cases and 417 GC cases. DEGs of GC were identified by "BiocManager" and "limma" R packages in R Studio (version R-4.3.3), and the details on cutoffs were as follows: $|\log FC| > 1.0$ and $p < 0.05$. The volcano plot and heat map of DEGs of GC were visualized by "ggplot2" and "pheatmap".

The Identification of Potential Gene Targets for HJD in GC Treatment

The potential active ingredients detected by UHPLC-Q-Orbitrap HRMS were selected if they met the following criteria: oral bioavailability (OB) ≥ 30% and drug-likeness (DL) ≥ 0.18 in the TCM Systems Pharmacology (TCMSP) (https://www.tcmsp-e.com/). The target genes of selected-active ingredients were obtained from the TCMSP and merged with the SwissTargetPrediction (http://www.swisstargetprediction.ch/) using a probability threshold of ≥ 0.1. The redundancies were removed. We uploaded the assembled targets to the UniProt database (https://www.uniprot.org/), confined the species to humans, and retrieved the official gene names for all targets. The potential therapeutic targets were then obtained from the intersection between the HJD targets and DEGs of GC by using the "VennDiagram" packages in R Studio (version R-4.3.3). The figure of the HJD-compound-targets network was drawn in Cytoscape (version 3.7.0).

The Characterization of Target Genes Associated with miRNA-21 in HJD Therapy for GC and Molecular Docking of miR-21-3p and p53

Using the miRWalk database (http://mirwalk.umm.uni-heidelberg.de/), we forecasted the potential downstream targets of miRNA-21, selected the therapeutic targets of HJD related to GC, and used Cytoscape (version 3.7.0) to visualize the target gene network for both miRNA-21. Sequences for miRNA-21-3p and p53 were obtained from miRBase (https://www.mirbase.org) and the National Center for Biotechnology Information website (https://www.ncbi.nlm.nih.gov/), respectively. These sequences were then input into the SWIEE-MODEL website (https://swissmodel.expasy.org) to identify the optimal protein structure. Nucleic acid-protein docking was performed on the Global Range Molecular Matching website (https://gramm.compbio.ku.edu/), and the docking model with the highest docking score was selected. Visualization of this model was achieved using Pymol (version 3.10).

Preparation of 5-Fu

The 5-Fu reagents needed for cell and animal experiments were prepared in a dark environment and were frozen at −20 °C and 4 °C, respectively, for use.

Cell Line and Cell Viability

The human GC cell line BGC-823 was obtained from Shanghai Genechem Co., Ltd. (Shanghai, China) on 5 November 2018, with approval from the Zhejiang Provincial Administration of TCM (approval number: 2022ZA056). Cells were cultured in RPMI-1640 medium (Hyclone, SH30809.01) supplemented with 10% FBS (Gibco, 10270–106) under standard culture conditions (37 °C, 5% CO_2). Cell viability was measured using the MTT assay, following the manufacturer's protocol. Cells in the logarithmic growth phase were seeded in 96-well plates at a density of 1×10^4 cells per well. After 24 h of incubation, BGC-823 cells were treated with various concentrations of 5-Fu (1.6–200 mg/L) for 72 h, different concentrations of HJD (0.4–6.4 mg/mL) for 24 h, and a combination of 5 mg/L 5-FU with increasing concentrations of HJD (0.2–6.4 mg/mL) for 24 and 48 h. Absorbance at 490 nm was measured using an enzyme labeler (Thermo, MA, USA), and growth curves were generated. Cell growth inhibition (IR) was calculated by using the following formula: $Cell\ growth\ inhibition(\%) = 100 \times \left(1 - \frac{OD\ value\ of\ experimental\ sample\ group}{OD\ value\ of\ control\ group}\right)$. The half-maximal inhibitory

 https://doi.org/10.2147/DDDT.S513371

concentration (IC_{50}) was calculated using GraphPad Prism 10 (Inc. La Jolla, CA, United States). All experiments were conducted in six replicate wells and repeated thrice.

Lentiviral Production and Infection

To produce a recombinant lentiviral vector expressing miRNA-21-3p, the complete miRNA-21-3p sequence was cloned downstream of human U6 (hU6) promoter in the plasmid backbone hU6-MCS-CBh-gcGFP-IRES-puromycin. For the control group, an unmodified phU6-MCS vector was used. BGC-823 cells were transduced with either control or miRNA-21-3p-targeting lentiviruses. After transduction, cells were selected with puromycin to establish two stable cell lines: a lentiviral negative control (vector) and a stable miRNA-21-3p knockdown line (miRNA-21-3p down). Cells were incubated at a temperature of 37 °C.

Group Division

Logarithmic-phase vector BGC-823 cells and miRNA-21-3p knockdown BGC-823 cells were harvested and divided into four groups: Control: RPMI-1640 + 10% FBS; 5-Fu: Control medium + 5 mg/L 5-Fu; HJD: Control medium + 1.62 mg/mL HJD; Combination: 5-Fu (5 mg/L) + HJD (1.62 mg/mL).

Colony Formation Assay

Vector BGC-823 cells and miRNA-21-3p knockdown BGC-823 cells were cultured in the conventional medium for 14 days after treatment according to the method described in Group Division for 72 h. Colonies were rinsed with 1×PBS (Gibco), fixed in a methanol acid solution at a 7:1 ratio, and stained using a 0.5% crystal violet solution. After a 1h incubation at room temperature, the staining solution was discarded, and the colonies were thoroughly washed and air-dried at room temperature. Mean values were calculated, and statistical analysis was performed using Analysis of Variance (ANOVA) with GraphPad Prism 10 (Inc. La Jolla, CA, United States).

Cell Migration Assay

The migratory ability of both vector BGC-823 cells and miRNA-21-3p knockdown cells was assessed using wound healing and transwell migration assays. For the wound healing assay, logarithmically growing cells were seeded in six-well plates at a density of 1×10^6 cells per well and incubated for 24 h in drug-free media. A wound was created using a 10-μL pipette tip, and the cells were treated according to Group Division for 24 h. Images were captured at 0 and 24 h to determine the migration rate by measuring the change in the cell-covered area. For the transwell migration assay, 24-well transwell plates with an 8-μm pore size membrane coated with Matrigel were used. A 100-μL suspension containing 2.0×10^5cells in serum-free medium was placed in the upper chamber, and cells were allowed to migrate toward the lower chamber containing 10% FBS medium at 37 °C for 24 h. Cells were treated according to Group Division, fixed with paraformaldehyde, stained with crystal violet (Solarbio, China), and photographed. The cell-covered area and number of migrating cells were quantified using ImageJ software (Media Cybernetics, Inc., Rockville, MD, USA). Mean values were calculated, and statistical analysis was performed using ANOVA with GraphPad Prism 10 (Inc. La Jolla, CA, USA).

Flow Cytometry (FCM)

Logarithmically growing vector BGC-823 cells and miRNA-21-3p knockdown BGC-823 cells were incubated overnight to achieve a cell density of 50–60% after 24 h. Cells were treated according to the methods outlined in Group Division for 48 hours, followed by Annexin-V/PI staining. Each experiment was repeated thrice. DNA content analysis was performed using ModFit LT software 5.0 (Verity Software House, USA) to determine the percentages of cells in the G_0/G_1, S, and G_2/M phases of the cell cycle. Mean values were calculated, and statistical analysis was performed using ANOVA with GraphPad Prism 10 (Inc. La Jolla, CA, United States).

Reverse Transcription Quantitative Polymerase Chain Reaction (RT-qPCR)

RNA was isolated using TransZol Up reagent (Invitrogen, Carlsbad, CA, USA), and its concentration and purity were determined using a Nanodrop One spectrophotometer (Thermo Fisher, USA). The cDNA was synthesized according to

the manufacturer's protocol using a reverse transcription kit. Subsequently, RT-qPCR was performed using the ChamQ Universal SYBR qPCR Master Mix (Vazyme, Nanjing, China) on a CFX96 Optics Module PCR system (Bio-Rad, Singapore). The relative gene expression was calculated by using the $2^{-\Delta\Delta CT}$ method. The p53, E-cadherin, and Vimentin mRNA levels were normalized by GAPDH. The miRNA-21-3p level was normalized by U6. The PCR primers were synthesized by the Sangon Biotech (Shanghai) Co., Ltd (Shanghai, China). The primer sequences were as follows: miRNA-21-3p RT primer: GTCGTATCCAGTGCAGGGTCCGAGGTATTCGCACTGGATACGACACAGCC, miRNA-21-3p forward: ACCGAGGTCAACACCAGTCGA, miRNA-21-3p reverse: ATCCAGTGCAGGGTCCGAGG; p53 forward: CAGCACATGACGGAGGTTGT, p53 reverse: TCATCCAAATACTCCACACGC; E-cadherin forward: GTCACTGACACCAACGATAATCCT, E-cadherin reverse: TTTCAGTGTGGTGATTACGACGTTA; Vimentin forward: TACAGGAAGCTGCTGGAAGG, Vimentin reverse: ACCAGAGGGAGTGAATCCAG; U6 RT Primer: GTCGTATCCAGTGCAGGGTCCGAGGTATTCGCACTGGATACGACAAAATA, U6 forward: AGAGAAGATTAGCATGGCCCCTG, U6 reverse: AGTGCAGGGTCCGAGGTATT; GAPDH forward: TGTAGACCATGTAGTTGAGGTCA, GAPDH reverse: GGTCGGGCAGGAAAGAGGGC. ANOVA was used for statistical analysis.

Western Blotting (WB)

Proteins were extracted in amounts of 15 μg and 60 μg from cellular and tissue lysates, respectively, and subsequently separated on a 10% SDS-PAGE gel using the Bio-Rad mini-PROTEAN electrophoresis system (Bio-Rad Laboratories, USA). Following electrophoresis, proteins were transferred onto PVDF membranes, which were incubated overnight at 4°C with primary antibodies targeting miRNA-21-3p, p53, E-cadherin, and Vimentin (all diluted 1:1000). The membranes were then incubated with secondary antibodies for 2 h at 4°C. Band intensities were analyzed and quantified using Quantity One software (Bio-Rad, USA). ANOVA was used for statistical analysis.

Tumor Xenograft Model in vivo

Animal experiments were approved by the Zhejiang Chinese Medical University's Laboratory Animal Research Center (IACUC-20220913-25) and conducted in accordance with China's national standards for laboratory animal welfare, including the Guidelines for Welfare and Ethical Guidance of Laboratory Animals (Ministry of Science and Technology) and the Regulations on the Administration of Laboratory Animals (State Council). Twenty 5-week-old female BALB/c-nu mice were used to establish a tumor xenograft model by subcutaneously injecting 100 μL of cell suspension containing 1.5×10^7 BGC-823 cells into their left forelimbs. The mice were housed in a controlled environment (23 ±2°C, 55 ±5% humidity, 12 h light-dark cycle) with standard laboratory food and water. When tumor volumes reached 100–300 mm^3, mice were randomized into four groups (n=5): blank control, 5-Fu, HJD, and synergistic group. Treatments were administered daily for 4 weeks: blank control (NS 0.1 mL/10 g i.p)., 5-Fu (5-Fu 0.1mL/10g, 2.5 mg/mL i.p)., HJD (HJD 0.1mL/10g, 0.39g/mL i.g)., and synergistic (5-Fu 0.1mL/10g, 2.5 mg/mL i.p. and HJD 0.1mL/10g, 0.39g/mL i.g). Tumor volume and body weight were measured thrice per week. Tumor volume was calculate using the formula: Tumor volume $= \frac{\text{longest diameter}\times\text{shortest diameter}^2}{2}$. After 4 weeks of treatment, the mice were euthanized under anesthesia, and tumors were excised for further analysis. ANOVA was used for statistical analysis.

Immunofluorescence (IF)

Metastasis-associated proteins in tumor tissue sections from tumor-bearing mice were analyzed using IF. Tumor slides were incubated overnight at 4°C with primary antibodies against E-cadherin, N-cadherin, and Vimentin (all diluted 1:1600). The following day, the slides were treated with a fluorescent secondary antibody (diluted 1:1600) and counterstained with DAPI (Abcam, Cambridge, UK). The stained sections were examined using the Olympus VS120-S6-W microscope (Olympus Corporation, Japan), and quantitative analysis was performed using ImageJ software (Media Cybernetics, Inc., Rockville, MD, USA). ANOVA was used for statistical analysis.

Statistical Analysis

All results were presented as mean ±standard error (SEM). Statistical analyses were conducted using GraphPad Prism 10 (Inc. La Jolla, CA, United States). Data were analyzed using ANOVA. $p < 0.05$ was considered statistically significant.

Results

Qualitative Analysis of Drug Components in HJD Based on UHPLC-Q-Orbitrap HRMS

The chemical composition of HJD was analyzed using the UHPLC-Q-Orbitrap HRMS system. Total ion chromatograms (Figure 2) revealed a complex chemical profile of HJD. A total of 639 components were detected in positive ion mode, while 298 components were identified in negative ion mode. The analysis indicated that HJD contains diverse compounds, including aromatic compounds, polysaccharides, flavonoids, chlorergic acids, and amino acids. Partial results of the mass spectrometry analysis are summarized in Table 1, with complete data providedin Supplementary File 1.

MiRNA-21 was Overexpressed in GC and Linked to Pathogenesis, Metastasis, and Clinical Stages

Through analysis of miRNA expression profiles from UCSC XENA, we identified 120 differentially expressed miRNAs in GC tissues compared to normal controls ($|logFC| > 1.0$, $p < 0.05$), including 102 upregulated and 18 downregulated miRNAs. Among these, miRNA-21 ranked as one of the top 18 most significantly upregulated miRNAs (Figure 3A and B). Further analysis demonstrated that high miRNA-21 expression was significantly associated with GC occurrence ($p < 0.0001$) and metastasis ($p < 0.05$), with stepwise overexpression observed from normal tissues to metastatic GC (Figure 3C). Additionally, miRNA-21 expression correlated with GC stage and tumor pathology (Table 2).

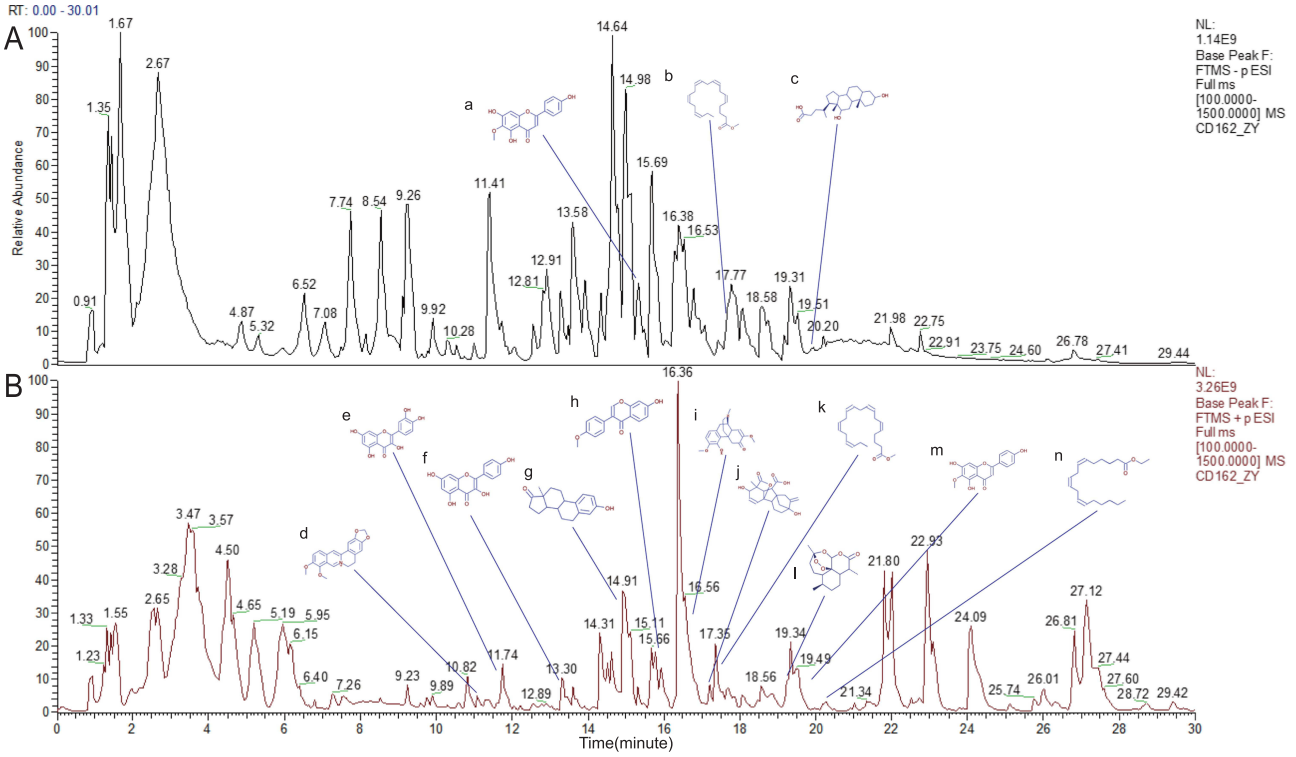

Figure 2 Total ion chromatogram of HJD obtained by UHPLC-Q-Orbitrap HRMS analysis in (**A**) positive ion mode and (**B**) negative ion mode. Peaks are annotated as follows: (a) 2-(2,4-dihydroxyphenyl)-3,5,7-trihydroxy-4Hchromen-4-one, (b) eicosapentaenoic acid methyl ester, (c) deoxycholic acid, (d) berberine, (e) quercetin, (f) kaempferol, (g) estrone, (h) 7-hydroxy-3-(4-methoxyphenyl)-4H-chromen-4-one, (i) sinomenine, (j) gibberellic acid, (k) arachidonic acid, (l) artemisinin, (m) hispidulin, (n) linolenic acid ethyl ester.

Table 1 Partial Presentation of the Results of HJD Mass Spectrometry

Name	Formula	m/z	RT [min]	Reference Ion	Area: CD162_ZY.raw (F1267)
L-Phenylalanine	C9 H11 N O2	166.08623	5.191	[M+H]+1	14398229470
Nicotinic acid	C6 H5 N O2	124.0394	2.116	[M+H]+1	330158598l
7-hydroxy-3-(4-methoxyphenyl)-4H-chromen-4-one	C16 H12 O4	269.08029	15.781	[M+H]+1	5496058024
Kaempferol	C15 H10 O6	287.05478	13.225	[M+H]+1	152140335.4
Quercetin	C15 H10 O7	303.04968	11.612	[M+H]+1	748384643.6
Linolenic acid ethyl ester	C20 H34 O2	307.263	20.771	[M+H]+1	72579787.21
Berberine	C20 H17 N O4	336.12274	11.388	[M+H]+1	339233709.6
Estrone	C18 H22 O2	293.14914	14.762	[M+H]+1	74879171.55
Sinomenine	C19 H23 N O4	330.16922	16.664	[M+ACN+H]+1	962187624.6
Artemisinin	C15 H22 O5	265.14331	15.398	[M+H]+1	242462137.6
Linoleic acid	C18 H32 O2	279.23257	22	[M-H]-1	1393951581
Palmitic Acid	C16 H32 O2	255.23262	22.513	[M-H]-1	262985287
Salicylic acid	C7 H6 O3	137.02304	12.767	[M-H]-1	968553404.9
Phenylacetaldehyde	C8 H8 O	119.04881	11.4	[M-H]-1	1381657377
Terephthalic acid	C8 H6 O4	165.0182	9.757	[M-H]-1	413845140.2
Chlorogenic acid	C16 H18 O9	353.08777	9.961	[M-H]-1	1436013651
16-Hydroxyhexadecanoic acid	C16 H32 O3	271.22772	19.285	[M-H]-1	113121510.7
Deoxycholic Acid	C24 H40 O4	391.28513	19.902	[M-H]-1	21707800.73
Arachidonic acid	C20 H32 O2	303.23264	21.919	[M-H]-1	707192163.1
Hispidulin	C16 H12 O6	299.05594	15.293	[M-H]-1	111275430.1

Functional Enrichment Analysis

We further investigated the functional enrichment of miRNA-21-related DEGs in GC. Patients with GC were stratified into two groups based on miRNA-21 expression levels using the "limma" R package ($|logFC| > 1.0$, $p < 0.05$): a high miRNA-21 expression group (2449 DEGs, Supplementary File 2) and a low miRNA-21 expression group (2271 DEGs, Supplementary File 3).

Functional enrichment analysis of these DEGs was summarized in Figure 4. For the high miRNA-21 expression group, GO analysis revealed enrichment in: (i) BPs: positive regulation of cell migration, extracellular matrix organization, integrin-mediated signaling pathway, and epithelial cell differentiation; (ii) CCs: extracellular space, focal adhesion, collagen-containing extracellular matrix, and cytoskeleton; and (iii) MFs: protein kinase binding, cadherin binding, protein serine/threonine kinase activity and actin binding (Figure 4A). In the low miRNA-21 expression group, GO analysis showed enrichment in: (i) BPs: intracellular signal transduction, positive regulation of cell migration, and actin cytoskeleton organization; in (ii) CCs: extracellular region, extracellular space, focal adhesion, and epithelial cell differentiation; and in (iii) MFs: adenosine triphosphate binding, cadherin binding, actin filament binding, and actin binding (Figure 4B). KEGG analysis indicated that DEGs in both groups were enriched in focal adhesion, peroxisome proliferator-activated receptor signaling pathway, and hypoxia-inducible factor-1 signaling pathway (Figure 4). Furthermore, both GO and KEGG analyses demonstrated that miRNA-21-related DEGs were associated with positive regulation of signal transduction by p53 class mediator, p53 signaling pathway, and cell cycle (Figure 4). These findings suggest that miRNA-21 be involved in GC metastatic behaviors, cell cycle regulation, and is associated with the p53 signaling pathway.

Active Targets of HJD Treating GC

To investigate the active targets of HJD in GC treatment, we analyzed GC-related DEGs from the UCSC XENA and GETx databases ($|logFC| > 1.0$, $p < 0.05$) and systematically collected potential therapeutic targets of HJD. The volcano plot illustrated the distribution of DEGs (Figure 5A). Heatmaps were generated to display distinct expression patterns of

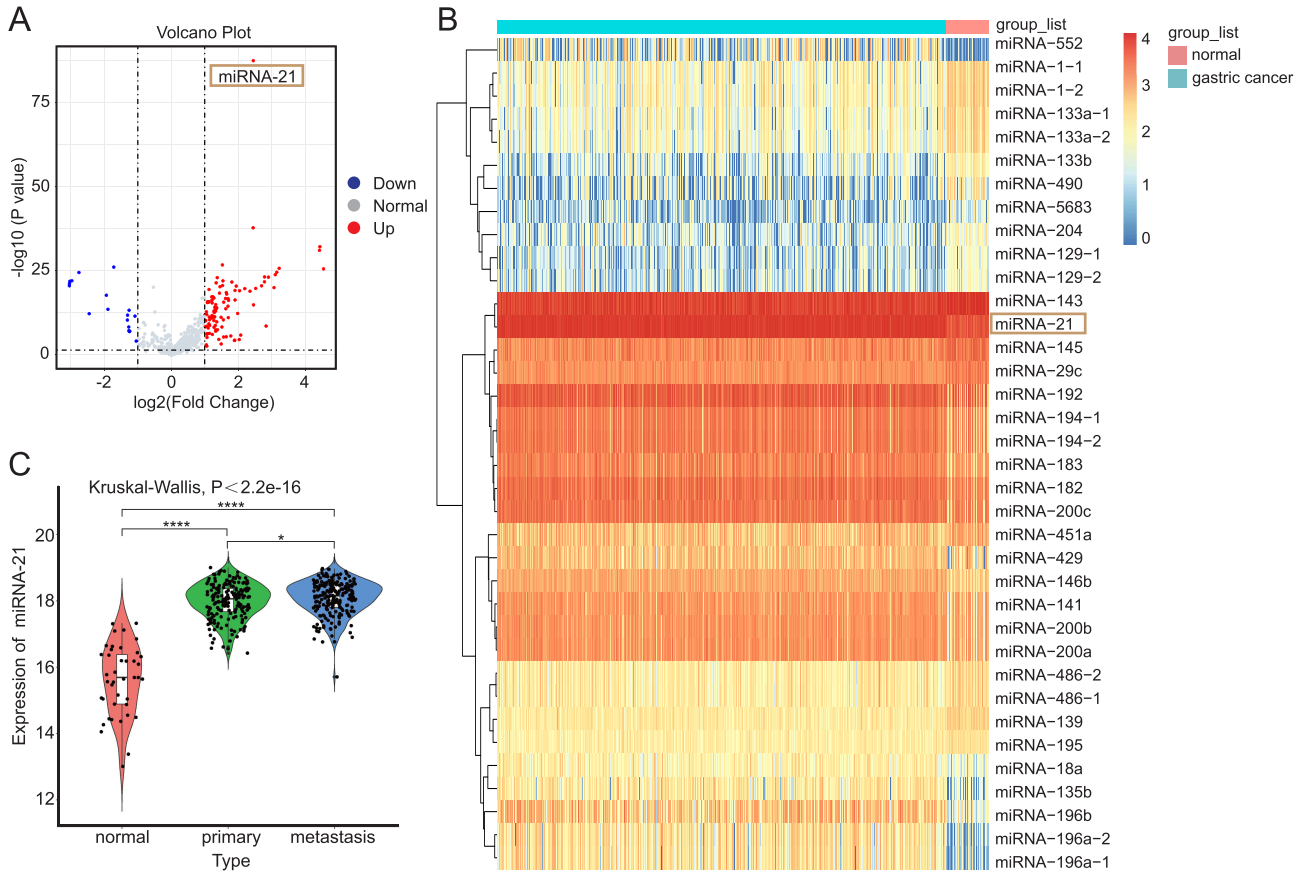

Figure 3 miRNA-21 is overexpressed in GC and associated with gastric carcinogenesis and metastasis. (**A**) Volcano plot of differentially expressed miRNAs in GC vs normal tissues (n=450: 40 normal; 410 GC). (**B**) Heatmap of the top 18 upregulated and downregulated miRNAs (n=450: 40 normal; 410 GC). (**C**) miRNA-21 expression in normal gastric tissues, primary GC, and metastatic GC tissues (n=433: 41 normal; 180 primary GC; 212 metastatic GC). *$p < 0.05$, ****$p < 0.001$.

upregulated and downregulated DEGs in GC (Figure 5B). To explore potential therapeutic targets of HJD in GC, active compounds in HJD were screened to identify 452 potential targets, and their corresponding targets were investigated. Following intersection analysis of DEGs with HJD-related targets, 162 overlapping targets were identified as potential therapeutic candidates (Figure 5C), and a network depicting HJD-compound-target interactions was constructed (Figure 5D).

Table 2 Correlations Between miRNA-21 Expression and Clinicopathology of GC

Parameter	No. of Cases	miRNA-21 Expression		*P*-value
		High	Low	
Gender	410			
Female	146	70 (47.9%)	76 (52.1%)	0.606
Male	264	135 (51.1%)	129(48.9%)	
Age	410			
<70	250	132 (52.8%)	118 (47.2%)	0.188
≥70	159	87(54.1%)	73(45.9%)	
Histological type	410			
Stomach adenocarcinoma	410	205(50%)	205(50%)	1
Other type	0	0 (0)	0 (0)	

(*Continued*)

Table 2 (Continued).

Parameter	No. of Cases	miRNA-21 Expression		*P*-value
		High	Low	
Neoplasm_histologic_grade	410			
G1	7	3 (42.9%)	4 (57.1%)	0.62
G2	145	68 (46.9%)	77(53.1%)	
G3	250	131(52.4%)	119 (47.6%)	
GX	8	3(37.5%)	5(62.5%)	
Lymph node metastasis	410			
0	38	14 (36.8%)	24(63.2%)	0.07
1–2	8	5 (37.5%)	3 (62.5%)	
3–6	43	16 (65.3%)	27 (34.7%)	
7 or more	321	170 (53.0%)	151(47.0%)	
Stage	410			
I	58	20 (61.8%)	38 (38.2%)	0.045
II	128	65 (60.7%)	63(39.3%)	
III	180	100(55.6%)	80(44.4%)	
IV	43	20(46.5%)	23(53.5%)	
Pathologic_M	410			
M0	362	180(49.7%)	182(50.3%)	0.771
M1	29	14(48.3%)	15(51.7%)	
MX	19	11(57.9%)	8(42.1%)	
Pathologic_N	410			
N0	137	61(44.5%)	76(55.5%)	0.557
N1	107	56(52.3%)	51(47.7%)	
N2	83	43(51.8%)	40(48.2%)	
N3	73	43(58.9%)	30(41.1%)	
NX		2(40%)	3(60%)	
Pathologic_T	410			
T1	20	6(30%)	14(70%)	0.001
T2	87	33(37.9%)	54(62.1%)	
T3	187	111(59.4%)	76(40.6%)	
T4	116	55(47.4%)	61(52.6%)	

MiRNA-21-3p/p53 is a Potential Therapeutic Pathway for HJD in GC Treatment

Target genes for miRNA-21-5p and miRNA-21-3p were also predicted, resulting in 51 and 109 overlapping genes with targets of HJD in the treatment of GC, respectively. According to the miRWalk database, the binding free energy between miRNA-21-3p and p53 was −20.9 kcal/mol, whereas that of miRNA-21-5p and p53 was −17.6 kcal/mol, indicating a stronger interaction of miRNA-21-3p with p53. After eliminating 47 duplicate genes, 113 unique target genes were identified, and a network diagram was constructed (Figure 6A). In this network diagram, the thickness of the connecting lines reflects binding energy strength (thicker lines for stronger binding), with miRNA-21-3p/p53 exhibiting a prominent thick line compared to the thinner miRNA-21-5p/p53 interaction. This visual and quantitative evidence supports the close association between miRNA-21-3p and p53, suggesting that miRNA-21-3p and p53 could be key potential targets for HJD in the treatment of GC.

We further generated a 3D binding model of miRNA-21-3p and p53 through homology modeling, and we generated 10 independent docking conformations. The optimal result was selected for presentation (Figure 6B), which exhibited a binding free energy of −37.3 kcal/mol. This predicted outcome suggests a robust interaction between miRNA-21-3p and p53, indicating a highly stable binding.

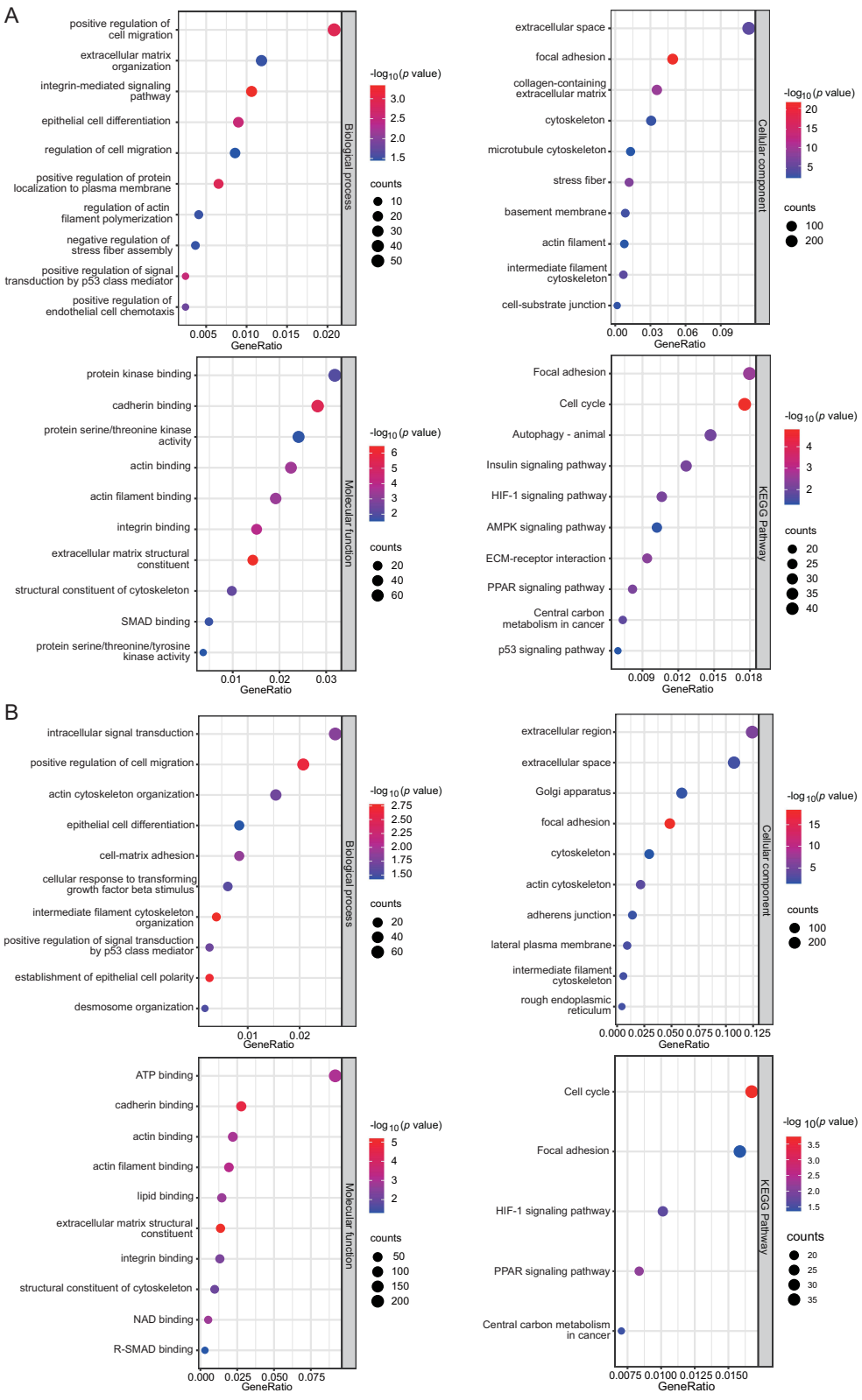

Figure 4 Gene Ontology (GO) and Kyoto Encyclopedia of Genes and Genomes (KEGG) analyses suggest miRNA-21 is associated with GC metastatic behaviors, cell cycle progression, and p53 pathway activity. (**A**) GO and KEGG enrichment analysis of miRNA-21-high-expressing differentially expressed genes (DEGs) in GC. (**B**) GO and KEGG enrichment analysis of miRNA-21-low-expressing DEGs in GC.

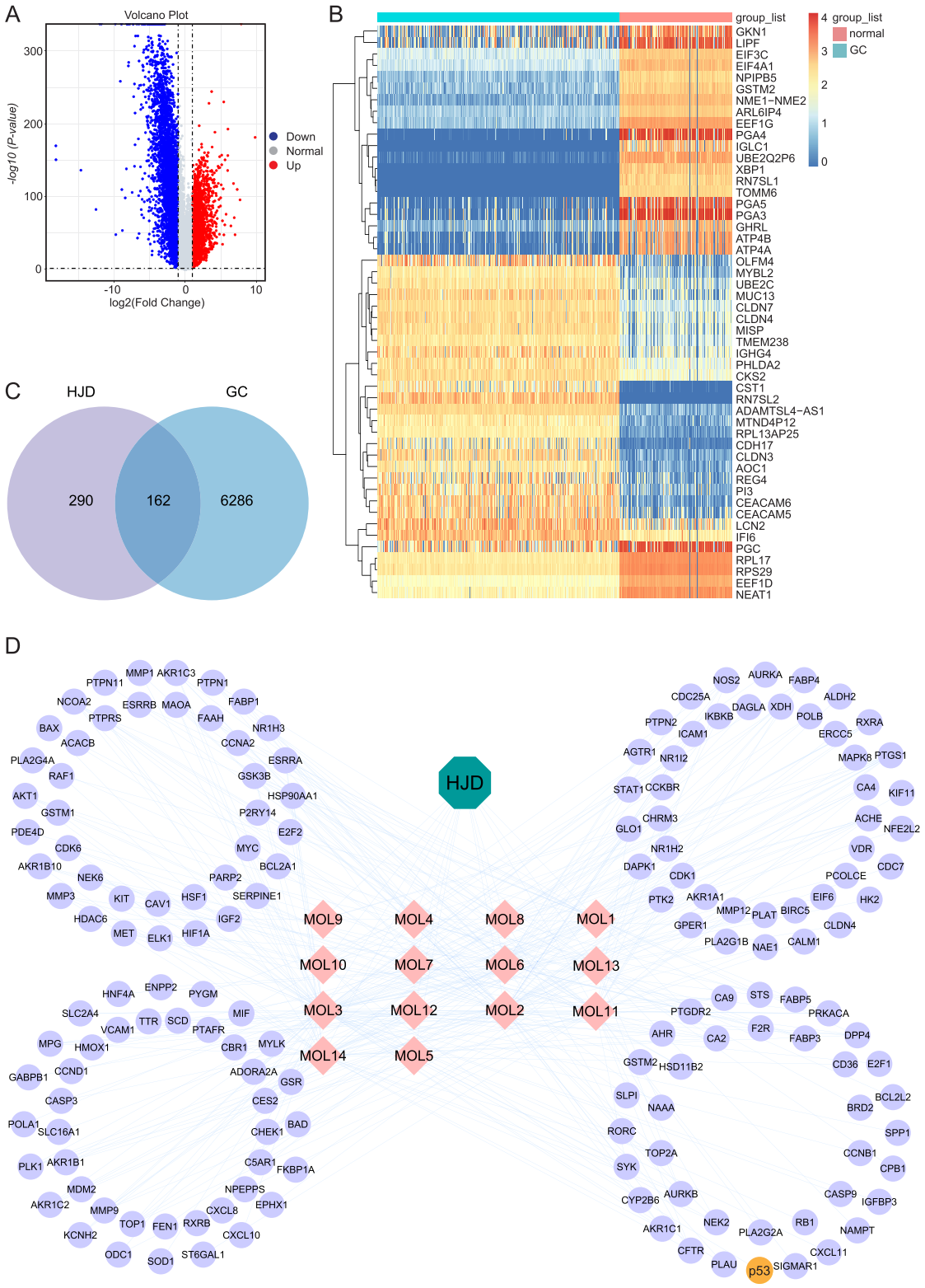

Figure 5 Identification of DEGs in GC using integrated data from the UCSC XENA and Genotype-Tissue Expression (GETx) databases, and prediction of potential therapeutic targets for HJD treatment. (**A**) Volcano plot of 6,508 DEGs in GC (n=500: 83 normal, 417 GC cases). (**B**) Heatmap displaying the top 25 upregulated and bottom 25 downregulated DEGs. (**C**) Venn diagram illustrating the intersection of HJD target genes with GC-associated DEGs, revealing 162 potential therapeutic targets. (**D**) Decoction-compound-target network for HJD: drug (hexagon), 14 active compounds (rhombus), and 162 targets (circle).

https://doi.org/10.2147/DDDT.S513371

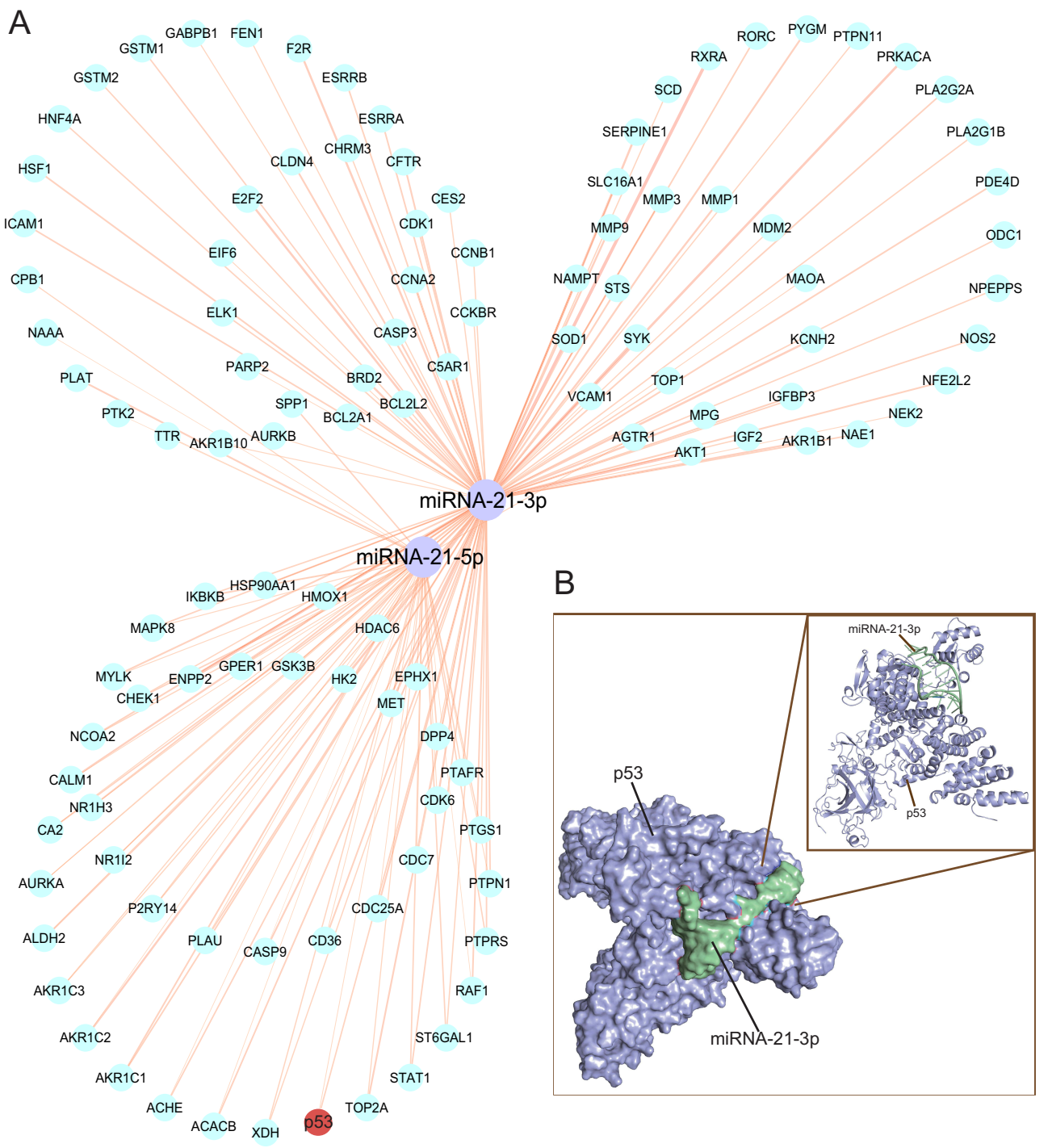

Figure 6 MiRNA-21-3p and p53 are proposed as potential key regulatory factors mediating the therapeutic effects of HJD in GC. (**A**) Network analysis of HJD target genes associated with miRNA-21-3p and miRNA-21-5p in GC treatment. Edge thickness correlates with interaction strength (thicker edges: stronger associations). (**B**) Molecular docking model illustrating the binding interface between miRNA-21-3p and p53.

The Inhibitory Effects of HJD Combined with 5-Fu on BGC-823 Cells

To evaluate the inhibitory effects of 5-Fu and HJD on BGC-823 cell proliferation, we analyzed their concentration-dependent growth suppression patterns. Both 5-Fu and HJD exhibited dose-dependent inhibition of cell viability (Figure 7A).

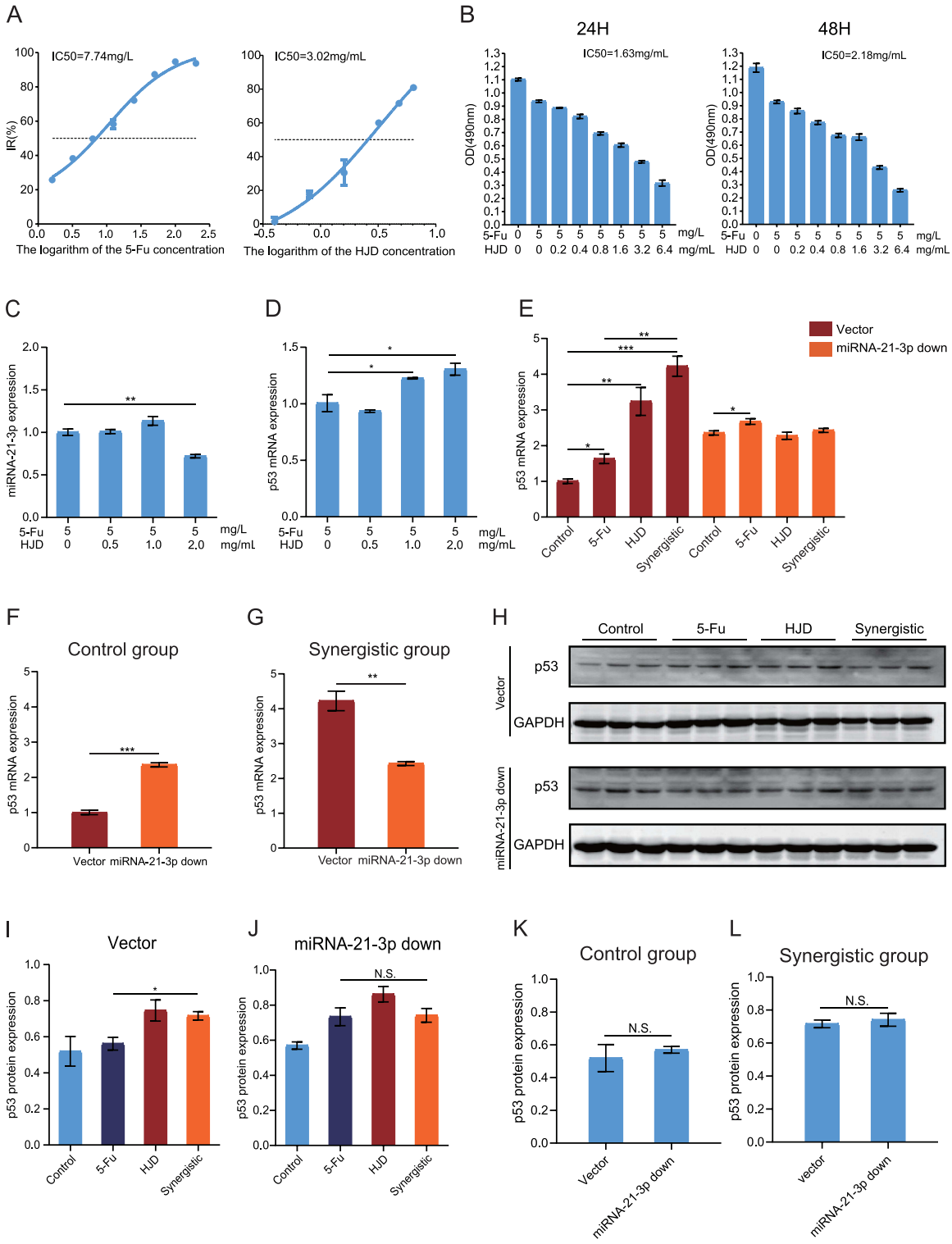

Figure 7 The cytotoxicity of HJD or 5-Fu on BGC-823 cells, the synergistic effect of HJD in combination with 5-Fu, and the preliminary validation of the miRNA-21-3p/p53 pathway. (**A**) Inhibitory effects of 5-Fu or HJD on BGC-823 cell growth (IC50: 7.74 mg/L for 5-Fu and 3.02 mg/mL for HJD, n = 6 per group). (**B**) Synergistic effects of HJD and 5-Fu on BGC-823 cell viability (MTT assay at 24 h and 48 h, n = 6 per group). (**C** and **D**) RT-qPCR analysis of miRNA-21-3p and p53 expression in BGC-823 cells treated with fixed 5-Fu and increasing HJD concentrations (n = 6 per group, ANOVA). (**E**) p53 mRNA levels (RT-qPCR) in BGC-823 cells with negative transfection or miRNA-21-3p knockdown across four groups: control, 5-Fu, HJD, and combination (n = 6 per group, ANOVA). (**F**) p53 mRNA expression (RT-qPCR) in control groups (negative transfection vs miRNA-21-3p knockdown, n = 6 per group, *t*-test). (**G**) p53 mRNA expression (RT-qPCR) in synergistic groups (negative transfection vs miRNA-21-3p knockdown, n = 6 per group, *t*-test). (**H–J**) p53 protein expression (Western blot) in BGC-823 cells with negative transfection or miRNA-21-3p knockdown (n = 6 per group, ANOVA). (**K**) p53 protein levels (Western blot) in control groups (negative transfection vs miRNA-21-3p knockdown, n = 6 per group, *t*-test). (**L**) p53 protein levels (Western blot) in synergistic groups (negative transfection vs miRNA-21-3p knockdown, n = 6 per group, *t*-test). Data: mean ± SEM. Statistical significance: **p* < 0.05, ***p* < 0.01, ****p* < 0.001, N.S. indicates no statistical significance.

https://doi.org/10.2147/DDDT.S513371

To assess the sensitizing effect of HJD on GC cells in response to 5-Fu, we investigated the combined inhibitory effect of varying concentrations of HJD (ranging from 0.2 to 6.4 mg/mL) with a fixed concentration of 5-Fu (5 mg/L) on BGC-823 cells (Figure 7B). In the control group without treatment, cell proliferation increased from 50% to 100%. Monotherapy with 5-Fu resulted in inhibition rates of approximately 15.66% and 22.77% at 24 and 48 h, respectively. However, the combination of increasing concentrations of HJD with a fixed concentration (5mg/L) of 5-Fu led to a continuous rise in the inhibition rate against BGC-823 cells. These initial findings suggest that HJD has the potential to significantly enhance the sensitivity of BGC-823 cells to 5-Fu.

HJD Enhances the Sensitivity of GC Cells to 5-Fu Through miRNA-21-3p/p53 Pathway

To experimentally validate whether HJD enhances 5-Fu sensitivity by modulating miRNA-21-3p and p53, BGC-823 cells were treated with increasing concentrations of HJD (0.5 to 2.0 mg/mL), and miRNA-21-3p and p53 expressions were measured via RT-qPCR. HJD significantly inhibited miRNA-21-3p expression at a concentration of 2.0 mg/mL ($p < 0.01$; Figure 7C) and increased p53 expression starting from a concentration of 1.0 mg/mL ($p < 0.05$; Figure 7D).

To investigate the interaction between miRNA-21-3p and p53 in mediating HJD's synergistic enhancement of 5-Fu-induced cytotoxicity in BGC-823 cells, we treated vector and miRNA-21-3p down cells as described in Group Division. In RT-qPCR analysis, p53 mRNA levels were significantly elevated in vector cells treated with HJD ($p < 0.01$) or the synergistic group ($p < 0.001$) compared to untreated controls (Figure 7E). The synergistic group exhibited higher p53 mRNA levels than 5-Fu monotherapy ($p < 0.01$; Figure 7E), and this upregulation was abolished in miRNA-21-3p down cells ($p > 0.05$; Figure 7E). Compared to the control group, miRNA-21-3p down cells alone significantly increased p53 mRNA expression ($p < 0.001$; Figure 7F). Furthermore, under co-treatment, p53 mRNA levels in vector cells were significantly higher than those in miRNA-21-3p down cells ($p < 0.01$; Figure 7G). Western blot analysis confirmed that the synergistic group induced a moderate but significant increase in p53 protein levels compared to 5-Fu alone in vector controls ($p < 0.05$; Figure 7H and I). Critically, this synergistic upregulation was completely abolished in miRNA-21-3p down cells ($p > 0.05$; Figure 7H and J). Although no statistically significant differences were detected, a consistent upward trend in p53 protein expression was observed in miRNA-21-3p down cells compared to vector cells across both control and synergistic groups ($p > 0.05$; Figure 7K and L). Although discrepancies in p53 expression were noted between RT-qPCR and Western blot results for the control and synergistic group, both assays consistently demonstrated that the synergistic enhancement of p53 expression (HJD+5-Fu vs 5-Fu alone) was abolished in miRNA-21-3p down cells. These findings conclusively support that HJD enhances the sensitivity of BGC-823 cells to 5-Fu via the miRNA-21-3p/p53 signaling pathway, thereby inhibiting cell proliferation.

HJD Augmented 5-Fu's Suppression of Colony Formation, Migration, and G_0/G_1 Cell Cycle Arrest Through miRNA-21-3p Regulation

To verify the synergistic effect of HJD with 5-Fu in inhibiting colony formation and migration of GC cells and to elucidate the underlying molecular mechanisms, we conducted colony formation, transwell, wound healing, and FCM assays on cells treated as described in Group Division.

In the colony formation assay, we observed that treatment in the synergistic group significantly reduced the colony-forming ability of vector BGC-823 cells compared to both the control and 5-Fu groups. However, the synergistic advantage over the 5-Fu group was eliminated following miRNA-21-3p knockdown ($p < 0.01$; Figure 8A and B). These results suggest that HJD may enhance 5-Fu's inhibitory effect on BGC-823 cell growth through miRNA-21-3p modulation.

The transwell assay demonstrated a stronger inhibitory effect on cell migration in the synergistic group compared to both the control and 5-Fu groups in vector cells ($p < 0.01$, Figure 8C and E). Additionally, HJD treatment effectively suppressed the migratory capability of vector BGC-823 cells ($p < 0.01$; Figure 8C and E). Upon miRNA-21-3p knockdown, the synergistic group showed a comparable inhibitory effect on migration to the 5-Fu group, while the HJD group failed to exhibit significant inhibitory activity (Figure 8C and F). The wound healing assay further supported these results, showing that the synergistic group significantly inhibited vector BGC-823 cell migration compared to both

the control ($p < 0.001$) and 5-Fu groups ($p < 0.001$; Figure 8D and G). However, in the case of miRNA-21-3p knockdown, no significant advantage in migration inhibition was observed in the combination treatment compared to 5-Fu alone (Figure 8D and H). These findings suggest that HJD enhances 5-Fu's inhibition of BGC-823 cell proliferation and migration through miRNA-21-3p regulation.

FCM analysis was performed to assess cell cycle distribution (Figure 8I). In vector BGC-823 cells, the synergistic group exhibited a significantly higher proportion of cells arrested in the G_0/G_1 phase compared to both the control ($p <$

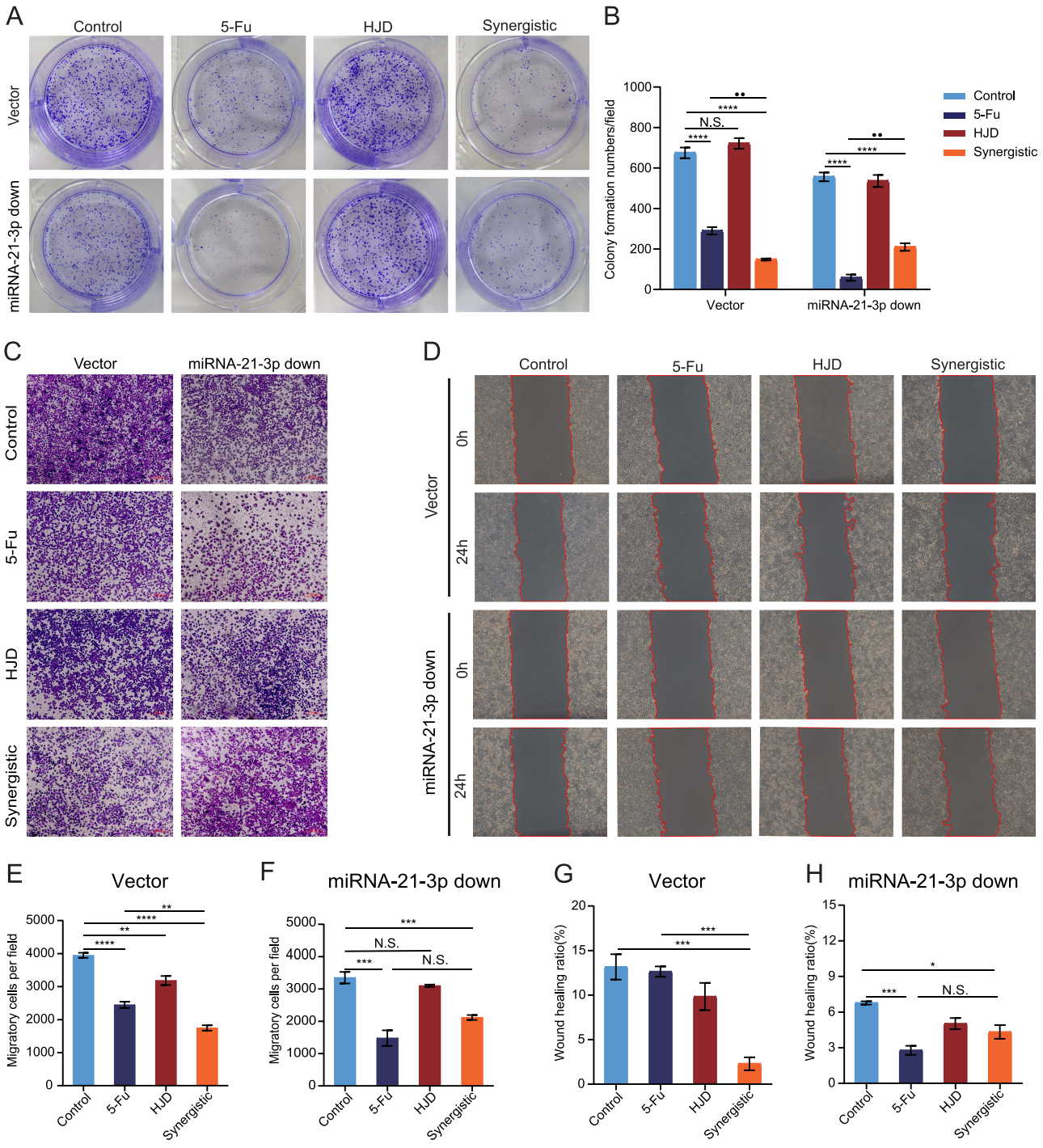

Figure 8 Continued.

https://doi.org/10.2147/DDDT.S513371

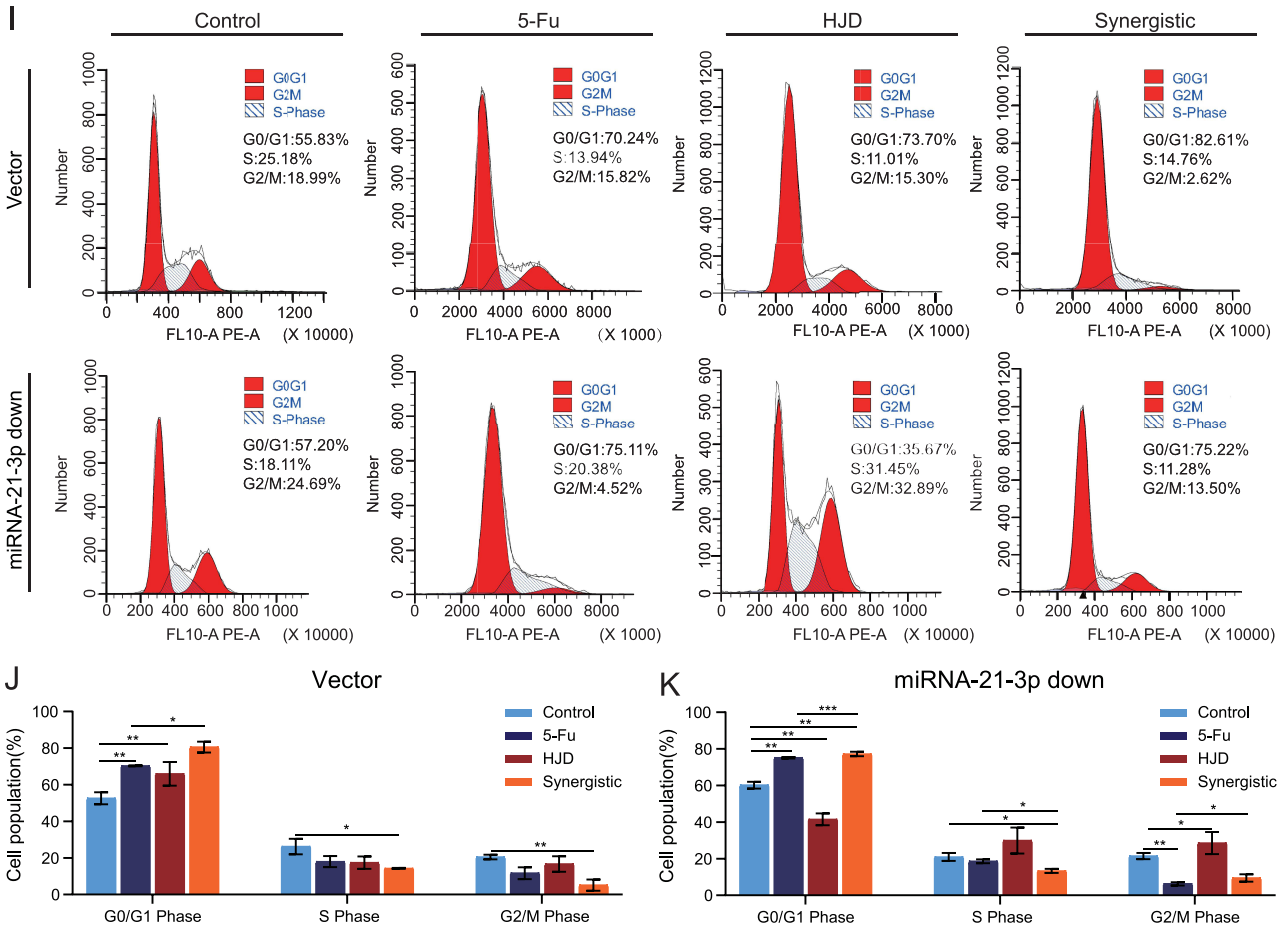

Figure 8 HJD synergizes with 5-Fu via miRNA-21-3p to suppress proliferation, migration, and G_0/G_1 phase arrest in BGC-823 cells. (**A** and **B**) Vector BGC-823 cells and miRNA-21-3p down from four groups (control, 5-Fu, HJD, and synergistic) were subjected to cell cloning assay (n = 6 per group). Quantification in panel B. (**C, E** and **F**) Transwell migration assay was conducted on the aforementioned groups. Quantification E and F (n = 6 per group). (**D, G** and **H**) Wound healing assay was conducted on the aforementioned groups. Quantification in G and H (n = 6 per group). (**I–K**) FCM assay was conducted on the aforementioned groups. Quantification in J and K (n = 5 per group). Data are presented as the means ±SEM. Values were tested by ANOVA. *$p < 0.05$, **$p < 0.01$, ***$p < 0.001$, ****$p < 0.0001$, N.S. indicates no statistical significance.

0.01) and 5-Fu groups ($p < 0.05$, Figure 8J). However, no substantial increase in G_0/G_1 phase arrest was observed between the synergistic and 5-Fu groups in miRNA-21-3p knockdown BGC-823 cells (Figure 8K). These results suggest that HJD may enhance G_0/G_1 phase arrest in BGC-823 cells through miRNA-21-3p regulation, contributing to its synergistic effect with 5-Fu.

The Combination of HJD and 5-Fu Enhanced Anti-Tumor Efficacy in vivo

To substantiate the inhibitory effect of HJD on GC tumors and its potential to enhance sensitivity to 5-Fu in vivo, we constructed a nude mouse model with subcutaneous tumors derived from BGC-823 cells. The combination group demonstrated the most pronounced inhibition, significantly surpassing the effects of the 5-Fu group ($p < 0.05$; Figure 9A and C). Tumor weight measurements obtained on the final day further confirmed the statistically significant inhibitory effect of the combination therapy on tumor growth ($p < 0.05$; Figure 9B). In terms of molecular effects, the expression of miRNA-21-3p was lowest in the HJD group, and the expression of miRNA-21-3p in tumor tissue was significantly reduced in the synergistic group compared to the 5-Fu intervention ($p < 0.0001$; Figure 9D). Additionally, the expression of p53 was higher in the synergistic group than in the 5-Fu group ($p < 0.05$; Figure 9E, G and H). E-cadherin expression was also upregulated in the synergistic group compared to both the control and 5-Fu groups (Figure 9F, G, I–K). Conversely, N-cadherin expression was significantly downregulated in the synergistic group relative

to both the control and 5-Fu groups (Figure 9F, J and K). Furthermore, Vimentin expression was significantly reduced in the synergistic group compared to the 5-Fu group (Figure 9F, G, J and K). However, WB analysis showed no statistically significant difference in Vimentin expression among the four groups (Figure 9I).

These findings suggest that HJD enhances 5-Fu sensitivity in GC tumors, potentially through the downregulation of miRNA-21-3p, upregulation of p53 and E-cadherin, and reduction of N-cadherin and Vimentin. While HJD alone demonstrated good biocompatibility, both 5-Fu monotherapy and combination therapy exhibited some degree of toxicity.

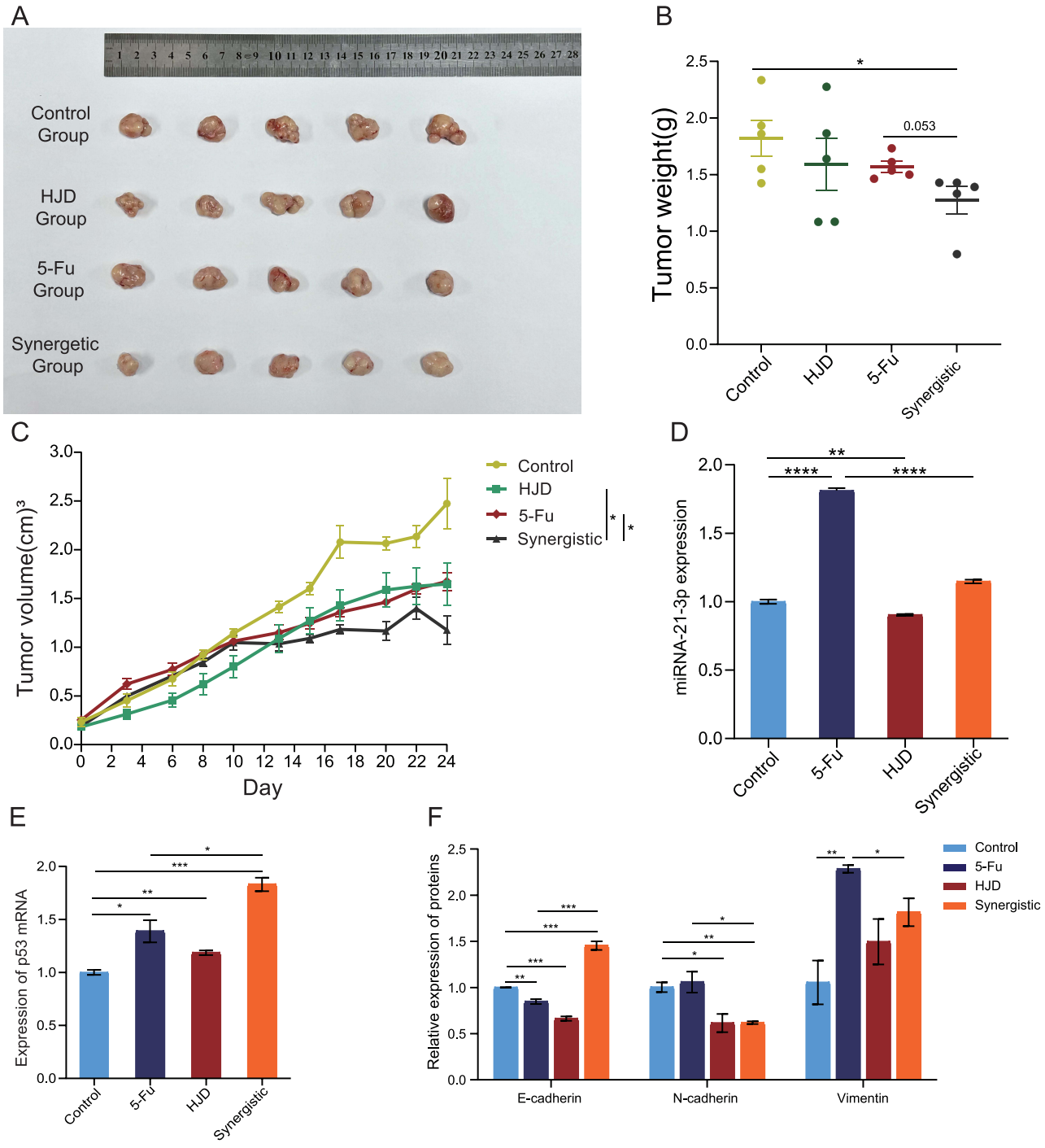

Figure 9 Continued.

https://doi.org/10.2147/DDDT.S513371

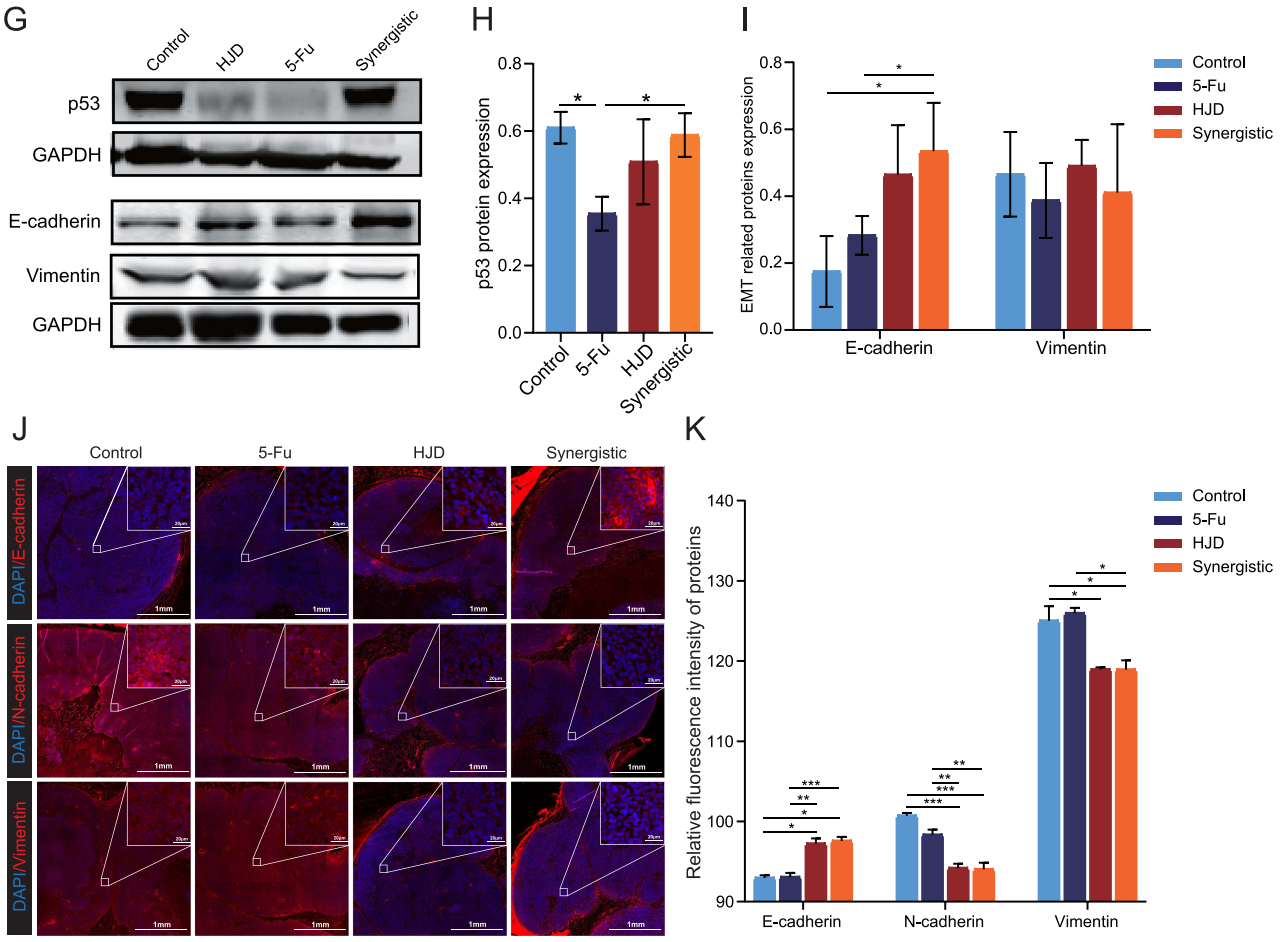

Figure 9 HJD, in combination with 5-Fu, inhibited GC proliferation and metastasis in vivo by modulating miRNA-21-3p downregulation and p53 upregulation. (**A**) The difference of mice tumor size in the four groups (control, 5-Fu, HJD, and synergistic) (n = 5 per group). (**B**) The tumor weight in the relevant groups at the end of the experiment (n = 5 per group). (**C**) The tumor volume of the relevant groups (n = 5 per group). (**D–F**) Relative expressions of miRNA-21-3p, p53, and E-cadherin, N-cadherin, and Vimentin in the tumor tissues of four groups were detected by RT-QPCR (n = 5 per group). (**G–I**) Protein expressions of p53, E-cadherin, and N-cadherin in the GC tissues of four groups were detected by WB (n = 5 per group). (**J**) Representative immunofluorescence images of E-cadherin, N-cadherin, and Vimentin in the GC tissues of mice (n = 5 per group). (**K**) Fluorescence intensity of E-cadherin, N-cadherin, and Vimentin in the GC tissues of mice of the aforementioned groups (n = 5 per group). The values were tested by ANOVA. *p <0.05, **p < 0.01, ***p < 0.001, ****p < 0.0001.

Discussion

GC remains one of the most prevalent malignant tumors of the gastrointestinal tract,[1] with China accounting for 44% of global cases.[16] By 2050, approximately 280,000 individuals in China are projected to be affected by GC annually.[16] Although 5-Fu adjuvant chemotherapy is widely used clinically, its efficacy is frequently limited by drug resistance,[17] a critical challenge demanding urgent solutions. In this context, TCM has emerged as a promising approach to enhance chemotherapy drug sensitivity.[18]

miRNA-21, significantly upregulated in various cancers including breast and lung cancers, is known to promote chemotherapy resistance.[19–21] Its role in GC has recently gained attention due to its overexpression correlating with aggressive tumor behavior.[22] Notably, Qi et al observed that 5-Fu paradoxically increases miRNA-21 expression in both serum and tumor tissues of GC patients, potentially contributing to therapeutic insensitivity.[23] Supporting this, nanoparticle-mediated suppression of miRNA-21 has been shown to enhance chemotherapeutic efficacy in GC.[24] The tumor suppressor p53, which regulates DNA repair, cell cycle control, apoptosis, and differentiation in GC,[25] is modulated by miRNAs such as miRNA-17-5p and miRNA-650.[26] Importantly, fluorescence and atomic force spectroscopy studies have confirmed the direct interaction between miRNA-21-3p and p53,[27] a relationship also observed in other tumors

where it inhibits cancer cell proliferation.[28,29] Building on these findings, our molecular docking analysis further predicted the binding interface between miRNA-21-3p and p53.

Our analysis of public databases revealed a significant correlation between elevated miRNA-21 expression and GC incidence and metastasis. GO and KEGG analyses further identified metastasis-related pathways among miRNA-21-associated DEGs. Crucially, we confirmed the miRNA-21-3p/p53 axis as central to HJD's dual mechanism of enhancing 5-Fu sensitivity and inhibiting GC progression, highlighting HJD's therapeutic potential. To characterize HJD's active components, mass spectrometry and network pharmacology identified six key compounds: kaempferol (inhibits proliferation via JAK2/STAT3 signaling,[30] and suppressing abnormal glycosylation[31]), sinomenine (targets miRNA-145-5p[32] and miRNA-204[33]), quercetin (binds p53,[34] induces ferroptosis[35] and pyroptosis,[36] reverses multidrug resistance[37]), berberine (acts through IL-6/JAK2/STAT3,[38] PI3K/Akt,[39] and PP2/GSK3β/MCL-1 pathways[40]), alongside deoxycholic acid and artemisinin (inhibiting H. pylori-associated carcinogenesis[41,42]).

These findings collectively suggest that HJD-5-Fu combination therapy may represent a potential therapeutic strategy. Mechanistically, HJD suppresses miRNA-21-3p to restore p53 activity, thereby sensitizing GC cells to 5-Fu. Unlike conventional therapies requiring sequential administration of synthetic inhibitors,[43,44] HJD's multicomponent synergy enables simultaneous target modulation. Notably, our observations revealed a discrepancy between p53 mRNA and protein expression patterns in vector BGC-823 cells versus miRNA-21-3p down BGC-823 cells. While miRNA-21-3p knockdown significantly elevated p53 mRNA levels (Figure 7F–G), Western blot analysis showed only non-significant protein upregulation (Figure 7K and L). This inconsistency may reflect the dual regulatory roles of miRNAs: canonical translational repression[45] and mRNA stability modulation.[46] We hypothesize that HJD-mediated miRNA-21-3p suppression in wild-type cells may stabilize p53 transcripts[47,48] while relieving translational inhibition,[45] whereas residual translational suppression[49] or rapid p53 protein turnover[50] could explain the attenuated protein response in knockdown cells. Critically, the complete abolition of HJD+5-Fu's synergistic p53 enhancement in miRNA-21-3p down BGC-823 cells (Figure 7E, I and J) reinforces the axis's mechanistic centrality.

While our in vitro and in vivo validations support this mechanism, preclinical studies must next compare toxicity profiles between HJD-5-Fu combinations and standard regimens (eg, 5-Fu/cisplatin-induced myelotoxicity).[51] Clinically, the miRNA-21-3p/p53 axis suggests two translational approaches: biomarker-guided HJD pretreatment to prime tumors for 5-Fu sensitivity, and dynamic HJD dosing during chemotherapy cycles based on serial miRNA-21-3p monitoring.

Several limitations warrant consideration. First, the observed mRNA-protein discordance in p53 expression underscores the need to explore post-transcriptional regulatory layers, such as RNA-binding protein interactions or ubiquitination dynamics, using techniques like ribosome profiling or pulse-chase assays, Second, while mechanistic validations were conducted in vitro, the absence of in vivo toxicity data (hepatorenal function, myelosuppression) necessitates other experiments and Phase I trials to establish HJD-5-Fu safety profiles. Third, the lack of in vivo validation using miRNA-21-3p-knockdown xenografts limits mechanistic confirmation in living systems. Fourth, Although BGC-823 cells exhibited the most pronounced miR-21-3p changes among four GC lines tested (SGC-7901, AGS, MKN-45), concerns about their cross-contamination status (eg, STR profiling discrepancies[52]) may limit result generalizability. Fifth, the unexplored role of miRNA-21-5p in HJD's mechanism requires further investigation.

Conclusion

This study reveals that HJD enhances 5-Fu sensitivity in GC by targeting the miRNA-21-3p/p53 axis. Through this mechanism (Figure 10), HJD induces G_0/G_1 cell cycle arrest, modulates EMT markers (E-cadherin, N-cadherin, and vimentin), and suppresses tumor proliferation/metastasis in cellular and animal models. The miRNA-21-3p-mediated chemosensitization indicates HJD's clinical utility as a biomarker-guided adjunct to 5-Fu regimens, specifically for miRNA-21-3p-overexpressing GC patients to improve chemotherapy efficacy and counteract resistance mechanisms. Collectively, these findings provide a preclinical foundation for exploring traditional medicine integration in precision oncology, particularly for advanced GC cases exhibiting miRNA-21-3p overexpression. Future studies should focus on reproducibility assessments in expanded sample cohorts, formulation optimization, mechanistic validation across heterogeneous tumor subtypes, and systematic evaluation of off-target effects prior to clinical translation.

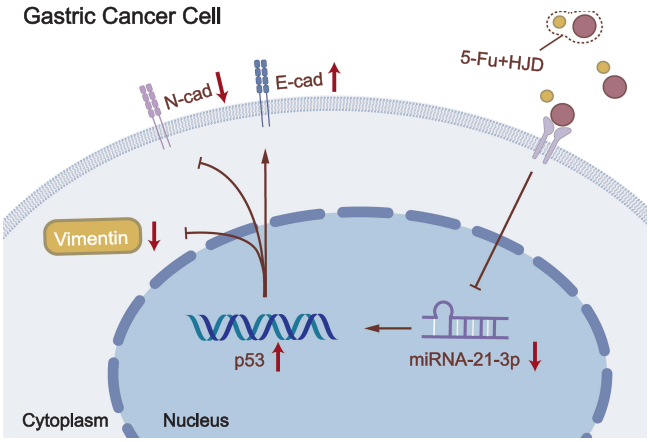

Figure 10 HJD increases the sensitivity of GC to 5-Fu, and the miRNA-21-3p/p53 pathway is involved.

Abbreviations

GC, Gastric cancer; HJD, Huashi Jiedu decoction; TCM, Traditional Chinese medicine; HD, Hedyotis diffusa Spreng; HP, Patrinia villosa Juss; HRA, Rabdosia amethystoides (Benth.) H.Hara; miRNA, microRNA; 5-Fu, 5-Fluorouracil; EMT, epithelial-mesenchymal transition; DEGs, differentially expressed genes; TCMSP, TCM Systems Pharmacology; ANOVA, analysis of variance; UHPLC-Q-Orbitrap HRMS, ultra-high performance liquid chromatography coupled with quadrupole-Orbitrap mass spectrometry; MTT, 3-(4, 5-Dimethylthiazol-2-yl)-2, 5-diphenyltetrazolium bromide; RT-qPCR, reverse transcription quantitative polymerase chain reaction; WB, Western blotting; FCM, flow cytometry; IF, immunofluorescence; AKT, protein kinase B; JAK2, janus kinase 2; STAT3, signal transducer and activator of transcription 3; NS, normal saline; OB, oral bioavailability; DL, drug-likeness; KEGG: Kyoto Encyclopedia of Genes and Genomes; GO, Gene Ontology. BPs, Biological Processes; CCs, Cellular Components; MFs, Molecular Functions.

Data Sharing Statement

The datasets used and analyzed during the current study are available from the corresponding author on reasonable request.

Ethics Approval and Consent to Participate

The animal experimental protocol was approved by the Laboratory Animal Research Center of Zhejiang Chinese Medical University (Approval No. IACUC-20220913-25). This study received exempt review approval from the Institutional Review Board (IRB) of The First Affiliated Hospital of Zhejiang Chinese Medical University, contingent upon the following prerequisites: (1) No deviations from or modifications to the research protocol shall be implemented without prior written authorization from the IRB; (2) Any proposed amendments to principal investigators, funding sources, protocols, informed consent documents, questionnaires, or recruitment materials must be submitted to the IRB through a formal protocol modification application, which will undergo re-evaluation.

Acknowledgments

We thank Mingjie Chen (Shanghai NewCore Biotechnology Co., Ltd.) for providing data analysis and visualization support. Revised Generative artificial intelligence(AI) Statement: In accordance with academic transparency standards, the authors disclose the implementation of generative AI technologies during the development of this research article. The Deepseek-R1 AI system was employed as an editorial tool to optimize linguistic precision and terminological consistency throughout the manuscript drafting process. Following AI-assisted modifications, all textual components underwent rigorous human evaluation and substantive editorial adjustments by the research team, which assumes complete accountability for the scholarly integrity and presentational quality of the finalized document.

This manuscript was previously uploaded as a preprint on SSRN (https://papers.ssrn.com/sol3/papers.cfm?abstract_id=4979750) – the paper has since been removed from the preprint server at our request.

Funding

This research was supported by Zhejiang Provincial TCM Scientific Research Fund Project (2022ZA056), and the Natural Science Foundation of Zhejiang Province (LY19H270005).

Disclosure

The authors report no conflicts of interest in this work.

References

1. Siegel RL, Miller KD, Wagle NS, Jemal A. Cancer statistics, 2023. *Ca Cancer J Clinicians*. 2023;73(1):17–48. doi:10.3322/caac.21763
2. Liu J, Yuan Q, Guo H, Guan H, Hong Z, Shang D. Deciphering drug resistance in gastric cancer: potential mechanisms and future perspectives. *Biomed Pharmacother*. 2024;173:116310. doi:10.1016/j.biopha.2024.116310
3. Zhu X, Lv J, Zhu M, et al. Development, validation, and evaluation of a risk assessment tool for personalized screening of gastric cancer in Chinese populations. *BMC Med*. 2023;21(1):159. doi:10.1186/s12916-023-02864-0
4. Chen Z, Yu T, Wang Y, Li J, Zhang B, Zhou L. Mechanistic insights into the role of traditional Chinese medicine in treating gastric cancer. *Front Oncol*. 2024;14:1443686. doi:10.3389/fonc.2024.1443686
5. Huang W, Wen F, Yang P, Li Y, Li Q, Shu P. Yi-qi-hua-yu-jie-du decoction induces ferroptosis in cisplatin-resistant gastric cancer via the AKT/GSK3β/NRF2/GPX4 axis. *Phytomedicine*. 2024;123:155220. doi:10.1016/j.phymed.2023.155220
6. Hu J, Bu W, Ding Y, et al. Jian pi hua tan fang reverses trastuzumab resistance of HER2-positive gastric cancer through PI3K/AKT/mTOR pathway: integrating network pharmacology, molecular docking and experimental validation. *Immun Inflamm Dis*. 2025;13(2):e70154. doi:10.1002/iid3.70154
7. Pang X, Shi C, Zhang L-Y, et al. Huashi jiedu decoction blocks cell cycle and inhibits EMT of gastric cells via LncRNA-p21. *Tradit Med Res*. 2023;8(12):67–72. doi:10.53388/TMR20230602001
8. Zhang H, Tang H, Tu W, Peng F. Regulatory role of non-coding RNAs in 5-fluorouracil resistance in gastrointestinal cancers. *Cancer Drug Resist*. 2025;8:4. doi:10.20517/cdr.2024.167
9. He Y, Hong Q, Chen S, Zhou J, Qiu S. Reprogramming tumor-associated macrophages in gastric cancer: a pathway to enhanced immunotherapy. *Front Immunol*. 2025;16:1558091. doi:10.3389/fimmu.2025.1558091
10. Chen Z, Zhang X, Li Z, Zhang H, Wang Z. lncRNA LINC02323 predicts adverse neoadjuvant chemotherapy outcomes of gastric cancer patients and regulates cell sensitivity to 5-fluorouracil by negatively modulating miR-139-3p. *Ann Med*. 2024;56(1):2424513. doi:10.1080/07853890.2024.2424513
11. Ding Y, Gao S, Zheng J, Chen X. Blocking lncRNA-SNHG16 sensitizes gastric cancer cells to 5-Fu through targeting the miR-506-3p-PTBP1-mediated glucose metabolism. *Cancer Metab*. 2022;10(1):20. doi:10.1186/s40170-022-00293-w
12. Xiang X, Ma HZ, Chen YQ, et al. GM-CSF-miRNA-Jak2/Stat3 signaling mediates chemotherapy-induced cancer cell stemness in gastric cancer. *Front Pharmacol*. 2022;13:855351. doi:10.3389/fphar.2022.855351
13. Hong Z, Li Y, Chen M, et al. Protosappanin B enhances the chemosensitivity of 5-fluorouracil in colon adenocarcinoma by regulating the LINC00612/microRNA-590-3p/Golgi phosphoprotein 3 axis. *Discov Oncol*. 2024;15(1):193. doi:10.1007/s12672-024-01036-7
14. Mei Y, Xu J, Li W, Chen S. Gambogic acid improves cisplatin resistance of bladder cancer cells through the epithelial-mesenchymal transition pathway mediated by the miR-205-5p/ZEB1 axis. *Ann Clin Lab Sci*. 2024;54(3):354–362. doi:10.18632/ONCOTARGET.15449
15. Li M, Cai O, Yu Y, Tan S. Paeonol inhibits the malignancy of apatinib-resistant gastric cancer cells via LINC00665/miR-665/MAPK1 axis. *Phytomedicine*. 2022;96:153903. doi:10.1016/j.phymed.2021.153903
16. He F, Wang S, Zheng R, et al. Trends of gastric cancer burdens attributable to risk factors in China from 2000 to 2050. *Lancet Reg Health West Pac*. 2024;44:101003. doi:10.1016/j.lanwpc.2023.101003
17. Gmeiner WH, Okechukwu CC. Review of 5-FU resistance mechanisms in colorectal cancer: clinical significance of attenuated on-target effects. *Cancer Drug Resist*. 2023;6(2):257–272. doi:10.20517/cdr.2022.136
18. Zhou C, Wu K, Gu M, Yang Y, Tu J, Huang X. Reversal of chemotherapy resistance in gastric cancer with traditional Chinese medicine as sensitizer: potential mechanism of action. *Front Oncol*. 2025;15:1524182. doi:10.3389/fonc.2025.1524182
19. Singh S, Saini H, Sharma A, Gupta S, Huddar VG, Tripathi R. Breast cancer: miRNAs monitoring chemoresistance and systemic therapy. *Front Oncol*. 2023;13:1155254. doi:10.3389/fonc.2023.1155254
20. Yang H, Liu Y, Chen L, et al. MiRNA-based therapies for lung cancer: opportunities and challenges?. *Biomolecules*. 2023;13(6):877. doi:10.3390/biom13060877
21. Chen SL, Hu D, Chen TZ, et al. Pan-cancer screening and validation of CALU's role in EMT regulation and tumor microenvironment in triple-negative breast cancer. *J Inflamm Res*. 2024;17:6743–6764. doi:10.2147/jir.S477846
22. Farasati Far B, Vakili K, Fathi M, Yaghoobpoor S, Bhia M, Naimi-Jamal MR. The role of microRNA-21 (miR-21) in pathogenesis, diagnosis, and prognosis of gastrointestinal cancers: a review. *Life Sci*. 2023;316:121340. doi:10.1016/j.lfs.2022.121340
23. Qi M, Liu D, Zhang S. MicroRNA-21 contributes to the discrimination of chemoresistance in metastatic gastric cancer. *Cancer Biomarkers*. 2017;18(4):451–458. doi:10.3233/cbm-161732
24. Hu N, Yin JF, Ji Z, et al. Strengthening gastric cancer therapy by trastuzumab-conjugated nanoparticles with simultaneous encapsulation of Anti-MiR-21 and 5-fluorouridine. *Cell Physiol Biochem*. 2017;44(6):2158–2173. doi:10.1159/000485955
25. Cai HQ, Zhang LY, Fu LM, Xu B, Jiao Y. Mutational landscape of TP53 and CDH1 in gastric cancer. *World J Gastrointest Surg*. 2024;16(2):276–283. doi:10.4240/wjgs.v16.i2.276

26. Lei ZN, Teng QX, Tian Q, et al. Signaling pathways and therapeutic interventions in gastric cancer. *Sig Transduct Target Ther*. 2022;7(1):358. doi:10.1038/s41392-022-01190-w
27. Moscetti I, Cannistraro S, Bizzarri AR. Probing direct interaction of oncomiR-21-3p with the tumor suppressor p53 by fluorescence, FRET and atomic force spectroscopy. *Arch Biochem Biophys*. 2019;671:35–41. doi:10.1016/j.abb.2019.05.026
28. Zhou Y, Guo D, Zhang Y. Association of MicroRNA-21 with p53 at mutant sites R175H and R248Q, clinicopathological features, and prognosis of NSCLC. *Mol Ther Oncolytics*. 2020;19:208–217. doi:10.1016/j.omto.2020.10.005
29. Luo X, Gu J, Zhu R, et al. Integrative analysis of differential miRNA and functional study of miR-21 by seed-targeting inhibition in multiple myeloma cells in response to berberine. *BMC Syst Biol*. 2014;8(1):82. doi:10.1186/1752-0509-8-82
30. Yang Y, Yuan L, Meng F, et al. Gancao xiexin decoction inhibits gastric carcinoma proliferation and migration by regulating the JAK2/STAT3 signalling pathway. *J Ethnopharmacol*. 2024;319(Pt 2):117241. doi:10.1016/j.jep.2023.117241
31. Radziejewska I, Supruniuk K, Tomczyk M, et al. p-Coumaric acid, kaempferol, astragalin and tiliroside influence the expression of glycoforms in AGS gastric cancer cells. *Int J Mol Sci*. 2022;23(15):8602. doi:10.3390/ijms23158602
32. Yan J, Yang J, Shen H, Gao R, Lv S. Sinomenine regulates circTRPM7-related pathway to inhibit gastric cancer cell growth and metastasis. *Chem Biol Drug Des*. 2023;102(4):870–881. doi:10.1111/cbdd.14297
33. Yuan H, Zhang J, Li F, Li W, Wang H. Sinomenine exerts antitumour effect in gastric cancer cells via enhancement of miR-204 expression. *Basic Clin Physiol Pharmacol*. 2019;125(5):450–459. doi:10.1111/bcpt.13285
34. Xu X, Yu Z, Zeng S. Investigating the therapeutic mechanism of xiaotan sanjie formula for gastric cancer via network pharmacology and molecular docking: a review. *Medicine*. 2023;102(46):e35986. doi:10.1097/md.0000000000035986
35. Ding L, Dang S, Sun M, et al. Quercetin induces ferroptosis in gastric cancer cells by targeting SLC1A5 and regulating the p-Camk2/p-DRP1 and NRF2/GPX4 axes. *Free Radic Biol Med*. 2024;213:150–163. doi:10.1016/j.freeradbiomed.2024.01.002
36. Rong Y, Liu SH, Tang MZ, Yang XJ. Quercetin inhibits the proliferative effect of gastric cancer cells by activating the pyroptosis pathway. *Asian J Surg*. 2023;46(11):5286–5288. doi:10.1016/j.asjsur.2023.07.051
37. Zhao G, Xue S. Mechanism of quercetin as a multidrug-resistant reversing compound in oxaliplatin-resistant gastric-cancer cell lines. *Alt Ther Health Med*. 2023;29(8):54–59.
38. Xu M, Ren L, Fan J, et al. Berberine inhibits gastric cancer development and progression by regulating the JAK2/STAT3 pathway and downregulating IL-6. *Life Sci*. 2022;290:120266. doi:10.1016/j.lfs.2021.120266
39. Liu Q, Tang J, Chen S, et al. Berberine for gastric cancer prevention and treatment: multi-step actions on the Correa's cascade underlie its therapeutic effects. *Pharmacol Res*. 2022;184:106440. doi:10.1016/j.phrs.2022.106440
40. Peng Z, Wangmu T, Li L, Han G, Huang D, Yi P. Combination of berberine and low glucose inhibits gastric cancer through the PP2A/GSK3β/MCL-1 signaling pathway. *Eur J Pharmacol*. 2022;922:174918. doi:10.1016/j.ejphar.2022.174918
41. Noto JM, Piazuelo MB, Shah SC, et al. Iron deficiency linked to altered bile acid metabolism promotes helicobacter pylori-induced inflammation-driven gastric carcinogenesis. *J Clin Invest*. 2022;132(10). doi:10.1172/jci147822
42. Su T, Li F, Guan J, et al. Artemisinin and its derivatives prevent helicobacter pylori-induced gastric carcinogenesis via inhibition of NF-κB signaling. *Phytomedicine*. 2019;63:152968. doi:10.1016/j.phymed.2019.152968
43. Zhang Z, Song W, Chen W, et al. Unveiling hotspots of emerging research in the miRNA-related mechanism underlying cancer through comprehensive bibliometric analysis with implications for precision medicine and non-invasive diagnostics. *Front Oncol*. 2024;14:1521251. doi:10.3389/fonc.2024.1521251
44. Li JW, Mao YM, Chen SL, et al. The interplay between metal ions and immune cells in glioma: pathways to immune escape. *Discov Oncol*. 2024;15(1):348. doi:10.1007/s12672-024-01229-0
45. Shang R, Lee S, Senavirathne G, Lai EC. microRNAs in action: biogenesis, function and regulation. *Nat Rev Genet*. 2023;24(12):816–833. doi:10.1038/s41576-023-00611-y
46. Rokavec M, Li H, Jiang L, Hermeking H. The p53/microRNA connection in gastrointestinal cancer. *Clin Exp Gastroenterol*. 2014;7:395–413. doi:10.2147/ceg.S43738
47. Capaccia C, Diverio S, Zampini D, Guelfi G. The complex interaction between P53 and miRNAs joins new awareness in physiological stress responses. *Cells*. 2022;11(10):1631. doi:10.3390/cells11101631
48. Feng Z, Liu J, Zhang C, Hu W. Chapter 4 - microRNAs and tumor suppressor p53 regulation. In: Negrini M, Calin GA, Croce CM editors. *MicroRNA Human Malignancies*. Academic Press; 2022:37–46. doi:10.1016/b978-0-12-822287-4.00001-3
49. Mosner J, Mummenbrauer T, Bauer C, Sczakiel G, Grosse F, Deppert W. Negative feedback regulation of wild-type p53 biosynthesis. *EMBO J*. 1995;14(18):4442–4449. doi:10.1002/j.1460-2075.1995.tb00123.x
50. Li Y, Wu M, Zhang L, et al. Nonsense-mediated mRNA decay inhibition synergizes with MDM2 inhibition to suppress TP53 wild-type cancer cells in p53 isoform-dependent manner. *Cell Death Discov*. 2022;8(1):402. doi:10.1038/s41420-022-01190-3
51. Connors J, Zhang L, Uryu H, et al. Distinct impact of platinum chemotherapies on the fitness and genome of hematopoietic stem cells and the risk of therapy-related myeloid neoplasms. *Blood*. 2024;144(Supplement 1):1816. doi:10.1182/blood-2024-212052